NORTHWESTERN UNIVERSITY

Surface Chemistry of Human-Derived Organic Compounds in Indoor Environments

A DISSERTATION

SUBMITTED TO THE GRADUATE SCHOOL IN PARTIAL FULFILLMENT OF THE REQUIREMENTS

for the degree

DOCTOR OF PHILOSOPHY

Field of Chemistry

By Jana Lee Butman

EVANSTON, ILLINOIS

September 2023

Abstract

Surface Chemistry of Human-Derived Organic Compounds in Indoor Environments

Jana Lee Butman

Thesis Advisors: Prof. Franz M. Geiger and Prof. Regan J. Thomson

Human skin oils are significant scavengers of atmospheric oxidants in occupied indoor environments. Many techniques used to study gas-phase transformations of surface films indoors have been limited to off-line bulk analysis, although more surface-selective methodologies are emerging. Here, we present a multi-prong analytical approach to characterizing skin oil ozonolysis. Skin oil is a complex heterogeneous system containing compounds like oleic acid and squalene, a major ozone-active constituent. We employ a combined spectroscopic and atomistic modeling approach to elucidate the conformational and orientational preferences of squalene at the air/oil interface and their implications for reactions with ozone. We find that squalene chains tend to align with surface normal, resulting in different concentrations of the various types of its double bonds at the interface and thus different reactivities. Skin oil and squalene are found to produce different vibrational sum frequency generation spectra in the C–H stretching region, while exposure to ozone results in surface spectra for both materials that is consistent with a loss of C–H oscillators. Measured contact angles show that the hydrophobicity of the films increases following exposure to ozone, consistent with the reduction in C═C···H_2O ("πH") bonding interactions that is expected from C═C double bond loss due to ozonolysis and indicating that the polar functional groups formed point toward the films' interiors. Further elucidation of skin oil's surface partitioning behaviors are revealed through mixing ratio studies of a binary squalene/oleic acid mixture. Implications for heterogeneous indoor chemistry are discussed.

Acknowledgments

Thank you first and foremost to Prof. Franz Geiger and Prof. Regan Thomson for co-advising this thesis. I would also like to thank my committee members, Prof. Karl Scheidt, Prof. Roel Tempelaar, and Prof. Richard Schaller for their guidance from the beginning to the end of my time here. I would also like to express my deepest thanks to my undergraduate advisor, Prof. Jerome Robinson. Without your mentorship and encouragement, I would have never believed myself capable of earning a PhD in chemistry. Alexandra Poterack, my advisor from the RISD Museum Guild, thank you so much for guidance as I developed my perspective on the Museum. Thank you to Dr. Eric Monroe at the Library of Congress for the constant support you have given me as I advance in this field. Thank you to Salomon Rodriguez from the student shop for providing your invaluable advice and input whenever I needed it. To Dr. Xinqi Chen of the Keck-II facility in NUANCE, thank you for the training and support as I gained expertise in optical profilometry.

Thank you so much to my Geiger cohort Emilie Lozier, Emily Ma, HanByul Chang, and my Thomson labmates Aidan Caravana, Israel Da Silva, Anhia Nguyen, Jenny Luo, and a special thank you to Aleia Bellcross for being both! I have learned so much from every single one of you and could not have made it this far without your collegiality and friendship. I would also like to thank past and present Geiger and Thomson lab members Ariana, Paul, Mavis, Rico, Cat, Johnny, Naomi, Hudson, Jen, Marvin, Amani, Raiden, Alyssa, Ezra, and anybody else who has answered a question, helped me find signal, or worked out a mechanism in group meeting. To my Northwestern Chemistry friends Zoha, Emily, Joanna, Brendan, and so many more people, thank you for the solidarity and the friendship. Dawning Liu, I cannot express how grateful I am for your friendship and mentorship. I learned so much about being a good scientist and spectroscopist from you, and your constant commitment to learning has filled me with admiration and inspiration.

Thank you to my family: my little brother, Alex Butman, and my parents, Dr. John Butman and Dr. Patty Lee. I would not have made it through the door without your love and support. To my best friend Kathryn Samp, thank you so much for the fun times, writing support, and for holding down the Kabana. To my friends Jake, Andrew, Phoebe, Kyle, Justin, Scott, and so many more, thank you so much for your friendship from near and far. To GCDED, this thesis would be of much higher quality and finished much sooner without you. To LDVD&D, thank you for the much-needed victories and no thank you for the undeserved defeats. I am extremely grateful for the support of my lovely girlfriend, Alexis, whose love and encouragement has helped more than I can express. I hope I can provide you with just as much support and motivation as you work towards your own doctorate. To my axolotl Xochi, you are my little god and miracle of science that has singlehandedly made this dissertation a reality.

List of Abbreviations

AFM	Atomic force microscopy
CIMS	Chemical ionization mass spectrometry
CCD	Charged-coupled device
IEPOX	Isoprene epoxydiol
IR	Infrared
MFC	Mass flow controller
ppb	Parts per billion
ppm	Parts per million
PTR	Proton transfer reaction
RH	Relative humidity
RMS	Root mean square
SFG	Sum frequency generation
SLP	Standard liter per minute
SOA	Secondary organic aerosol
Sq	Root mean square height
STP	Standard temperature and pressure
Tg	Teragrams
ToF	Time of Flight
TOPAS	Tunable optical parametric amplifier setup
UHV	Ultra-high vacuum
UV	Ultraviolet
VOC	Volatile organic compound

Table of Contents

List of Figures

List of Tables

Chapter 1:

Surface Analysis in Indoor Atmospheric Chemistry

Portions of this chapter appear in the following publications:

von Domaros, M.; Liu, Y.; **Butman, J. L.;** Perlt, E.; Geiger, F. M.; Tobias, D. J., Molecular Orientation at the Squalene/Air Interface from Sum Frequency Generation Spectroscopy and Atomistic Modeling. *The Journal of Physical Chemistry B* **2021**. *125* (15), 3932-3941

Butman, J. L.; Thomson, R. J.; Geiger, F. M., Unanticipated Hydrophobicity Increases of Squalene and Human Skin Oil Films Upon Ozone Exposure. *J Phys Chem B* **2022**, *126* (45), 9417-9423

1.1 Introduction

Whether at home or at work, North Americans spend the vast majority (90%) of their time indoors.[1] This behavior can be problematic, as the concentration of certain air pollutants can be 2 to 50 times higher indoors than outdoors. Indirect evidence supports connections between high levels of pollutants found indoors and morbidity (chronic fatigue syndrome, asthma, sick building syndrome) and even mortality.[2-4] Surface to volume ratios indoors far exceed that of the outdoors, [5] making surface chemistry disproportionately important in understanding pollutants. Through processes collectively referred to as "sorption", surfaces regulate physical and chemical transformations that gas-phase species undergo indoors.[6-8] Numerous methods exist for evaluating the bulk properties of indoor environments, but surface analysis requires specific methodologies. We attempt to bridge the existing knowledge gap in indoor surface chemistry using vibrational spectroscopy combined with optical profilometry, contact angle measurements, and other surface characterization techniques.

1.2 Molecular-Level Analysis in Indoor Surface Chemistry

Understanding the interaction of sorbed surface species with gas-phase reactants indoors is critical to understanding the subsequent impacts of indoor air pollution on human health through dermal uptake and inhalation.[9-19] Recent molecular-level studies on the surface processes of indoor environments provide microscopic and mechanistic insights into these heterogeneous chemical transformations.[20-36] These surface processes we define as the interaction of the topmost layer of molecules in direct contact with the gas phase, with a micrometer-thick bulk phase beneath an Angstrom to nanometer-thin surface. From atmospheric aerosol studies, we have learned that RH (relative humidity) governs the diffusivity between the surface and bulk, making the bulk accessible to incoming reactants in a humid environment. [35-38] At a low RH, the viscosity and diffusivity in a sorbed film is inhibited, endowing the topmost surface layer with a larger role in gas-phase interactions. The

responsivity of thin surface films to environmental conditions indicates a need for surface analysis that can be performed in ambient conditions. Methods requiring ultra-high vacuum (UHV), elevated temperature, and other deviations from standard indoor conditions can reveal useful information but are ultimately observing nontypical systems.

Current state of the art chemical analysis of collected surface films indoors often include experiments that are performed off-line and require solvent extraction, divorcing the studied systems of interest from the original conditions at which they need to be understood.[41, 51-53] Solvent extraction can lead to material loss of low-solubility compounds at the site of collection as well as material loss of low-volatility compounds in transportation and sample reconcentration. Similar off-line approaches run the additional risk of scrambling the surface and bulk phase components, limiting accuracy regarding actual indoor pollutant behavior. Sample collection for these approaches is often restricted to longer time scales, with collection windows ranging from hours to months. Specific surface processes that can be monitored on-line at faster time resolutions are therefore necessary to understand fast heterogeneous processes like ozonolysis.

1.3 The Impact of Human Occupation and Ozonolysis on Indoor Air

Numerous studies exist for both on- and offline analysis of indoor air pollutants that evolve due to human occupancy, with model environments ranging from closed airplane cabins to classrooms.[37] These studies point to a common conclusion: that human occupancy immediately changes the composition of an indoor space, on a time scale of seconds. Bulk measurements like on- and offline MS analysis show a rapid increase in human-derived VOCs (volatile organic compounds, e.g. exhalants like acetone and CO_2) the longer a subject remained in an observed enclosed area.[37-38] Human occupants significantly impact indoor air composition directly through breath and skin emissions.[37, 39-41] Indirectly, human presence causes a similarly significant impact due

to skin oil acting as a source/sink for gas-phase indoor reactants, leading to the formation of secondary VOCs (sVOCs) that further alter the chemistry of an indoor environment.

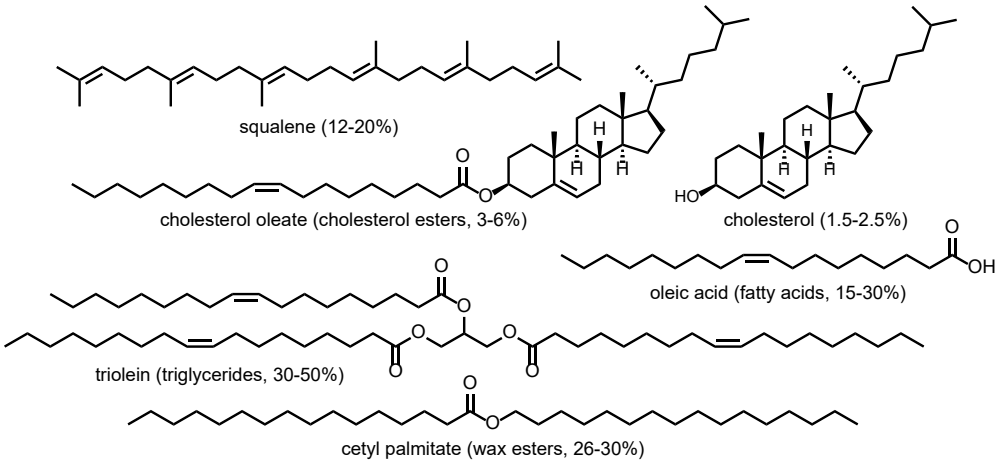

Figure 1.1: Major components of skin oil with structures of representative molecules and percentages

Much focus has been paid to the interaction of ozone with the components of human skin oil, in part due to the proximity of evolved sVOCs to critical mucous membranes and inhalation sites. The C=C double bonds of unsaturated lipids in skin oil can react heterogeneously with ozone on various surfaces such as skin, hair, soiled clothing, and any other indoor surface including shed skin flakes and deposited skin oil, processes known collectively as "desquamation." These reactions immediately lower the ozone concentrations in occupied indoor environments and generate a variety of (di)carbonyls, carboxyls, and hydroxycarbonyls, some of which have been identified as lung and skin irritants as shown in Figure 1.2.[37, 41]

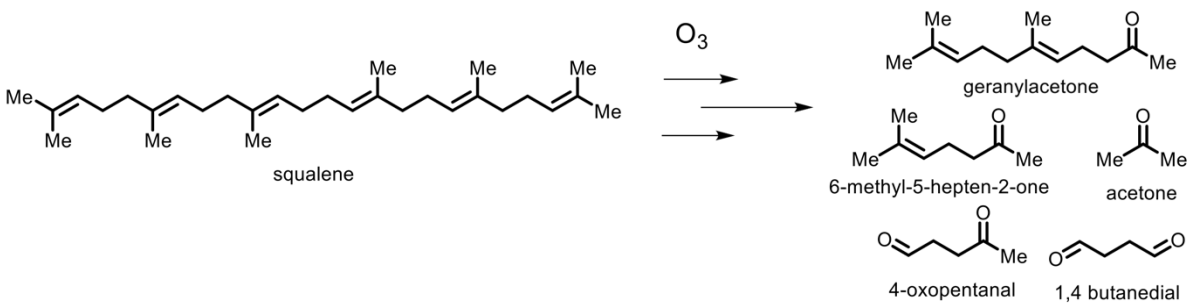

Figure 1.2: Chemical structures of squalene and select ozonolysis products.

Studying the surface properties of the heterogeneous reaction of ozone with human skin oil is critical to understanding the ultimate impact of indoor air pollution on human health. The speed of the reaction necessitates fast on-line analytical methodology. The collision of an ozone molecule with a C=C double bond is needed to start the reaction, as shown in Figure 1.3. Deconvoluting the surface orientation of a C=C bond containing skin oil molecule would therefore provide insight regarding the surface-gas interaction involved in initiating ozonolysis of skin oil.

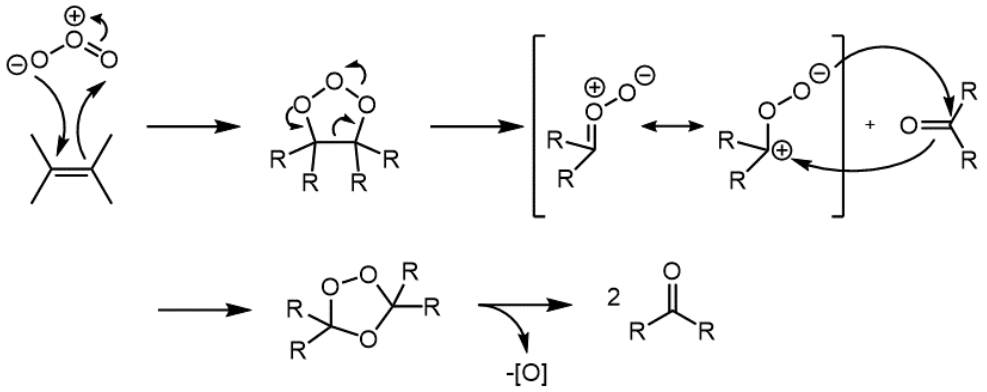

Figure 1.3: General mechanism for the ozonolysis of a C=C bond

1.4 Thesis Scope and Organization

In this introduction, we present an overview of the field of indoor air pollution's impact on human health and identify some of the current shortcomings regarding the analytical methods used to characterize atmospherically relevant surfaces. We identify challenges in the field of indoor surface characterization including the need to perform surface-specific analysis at ambient temperature and pressure, as well as the difficulty of obtaining on-line data of heterogeneous surface transformations. A knowledge gap exists regarding heterogeneous transformations occurring between ozone and skin oil components, which must be understood at the molecular surface level to understand their subsequent effects on human health. Our efforts to close this gap include probing environmentally relevant surfaces under ambient conditions using vibrational sum frequency generation (SFG)

spectroscopy paired with atomistic modeling, investigating surface properties using optical microscopy and contact angle measurements, and mixing studies using multicomponent model systems.

In Chapter 2, an investigation of molecular orientation at the squalene/air interface is performed using vibrational SFG spectroscopy under ambient conditions. Further morphological information about squalene films on silica is obtained using optical profilometry. Combining this experimental surface-selective approach with atomistic modeling reveals important implications for squalene ozonolysis products and rates.

Chapter 3 covers the effects of ozonolysis on the surface properties of skin oil and squalene films using SFG spectroscopy, contact angle measurements, and optical profilometry. The final section of chapter 3 details preliminary on-line kinetic observation of skin oil ozonolysis including bond-specific data obtained using SFG spectroscopy.

Chapter 4 covers preliminary surface studies of a two-component model system comprised of oleic acid and squalene observed using SFG spectroscopy and bulk scattering. The appendix will cover additional characterization of organosulfate atmospheric VOCs using SFG spectroscopy.

Chapter 2:

Surface Investigation of Squalene

Portions of this chapter appear in the following publications:

von Domaros, M.; Liu, Y.; **Butman, J. L.;** Perlt, E.; Geiger, F. M.; Tobias, D. J., Molecular Orientation at the Squalene/Air Interface from Sum Frequency Generation Spectroscopy and Atomistic Modeling. *The Journal of Physical Chemistry B* **2021**. *125* (15), 3932-3941

2.1 Introduction

Among the many heterogeneous reactions that are relevant for the chemistry of the indoor environment, much attention has focused on the oxidation of unsaturated organic compounds by ozone.[3] Specifically, ozone can react with the C=C double bonds in skin oil constituents, forming volatile lung irritants.[37] Since these constituents are amply available on skin, clothing, and other indoor surfaces, these irritants are formed in very close proximity to the respiratory system.[42] Models of skin oils have largely focused on commercially available unsaturated compounds, like squalene and oleic acid.[43-48] These choices are reasonable: due to the abundance of its C=C double bonds, squalene constitutes about 50% of the ozone-reactive species,[37] even though it comprises only about 10% of human skin oil. The remainder of human skin oil is comprised of saturated fatty acids which contain only one C=C double bond (e.g., oleic acid),[37] and unsaturated or saturated compounds like triglycerides. Much work has focused on the ozonolysis of these C=C double bonds as the process can lead to the formation of 4-oxopentanal, acetone, and other known lung irritants, particularly in close proximity to the human respiratory system.[38, 42, 49-50] The impact that skin oil has on the indoor atmosphere is not limited to durations of human occupation. Deposited skin oil, shed skin flakes, and other off-body, desquamated material also act as a significant sink for ozone indoors.[51] We focused our research on the properties of these desquamated samples, selecting silica (SiO_2) as a substrate, as it has been used as a model system for window glass, a common indoor surface, in several studies previously.[30]

2.2 Methods

2.2.1 Materials

Samples were prepared by dissolving squalene (Sigma-Aldrich, Part No. S3626, >98%, used as received) in deuterated chloroform, $CDCl_3$ (Sigma-Aldrich, Part No. 151823, 99.8 atom % D), and

spin-coating squalene at 3000 rpm onto a fused silica optical window substrate (ISP Optics, Part No. QI-W-25-3) that had been sonicated in methanol (Fisher Scientific, Part No. A452-4, HPLC grade), rinsed with methanol and Millipore water alternately, and then plasma cleaned. Skin oil samples were obtained from one human who did not use personal care products on the day of sampling. Following the method published by the Abbatt group,[52] the subject swiped their thumb over their forehead once and deposited the collected skin oil onto a fused silica window, smearing the oil to create a thin film. The coated sample window was clamped vertically on a translational stage. The ambient temperature and relative humidity in the laboratory were maintained at 20 ± 1 ºC and 30 – 50%, respectively.

2.2.2 Vibrational Sum Frequency Generation (SFG) Spectroscopy

Previously, squalene's bulk and surface properties had been studied using many of the methods outlined in Section 1.2, although SFG characterization did not yet exist in the literature. Second-order nonlinear vibrational spectroscopy allows for surface-selective chemical characterization, as bulk responses to the spectra are forbidden by symmetry arguments, and the technique is applicable at ambient pressure and temperature,[53-56] avoiding the pitfalls of other methods that require heat or ultra-high vacuum (UHV). Using SFG, we can obtain bond-specific and surface-selective chemical information.

SFG spectroscopy relies on a second-order process that occurs when two light fields overlap spatially and temporarily at an interface and generate an output light field that oscillates at the sum frequency of the two incident fields. The intensity of the output SFG signal is proportional to the effective second-order susceptibility, $\chi_{eff}^{(2)}$, of the interface. At the surface of an organic film, the nonresonant component of the term $\chi_{eff}^{(2)}$ is generally small when compared to the resonant contribution. The resonant component can be written as

$$\chi_R^{(2)} = N < \beta_{ijk,q} > \quad (1)$$

where N is the number of interfacial molecules and $< \beta_{ijk,q} >$ is the orientational ensemble average of the molecular hyperpolarizability tensor. For each normal mode *q*, $\beta_{ijk,q}$ is proportional to the product of the derivatives of both the polarizability, α_{ij}, and dipole moment, μ_k, with respect to the normal mode coordinate, Q_q.

$$\beta_{ijk,q} \propto \frac{\partial \alpha_{ij}}{\partial Q_q} \frac{\partial \mu_k}{\partial Q_q} \quad (2)$$

The polarization-resolved SFG signal is sensitive to the orientations of vibrational modes, which can help us deduce the orientation of the chemical bonds and even the entire molecule. Such an approach has seen many successful precedents in interfacial chemistry in various contexts, which provides a rich library aiding in spectral assignment and orientational analysis, especially in the C–H stretching region.[57-61]

SFG spectroscopy can probe the functional groups on surfaces nondestructively under ambient conditions in an online manner with time resolution of sub-seconds. Moreover, SFG spectroscopy is intrinsically surface selective because SFG signal is generated through a nonlinear optical process where centrosymmetry is broken and thus amorphous bulk media inherently remain silent. Our broadband vibrational sum frequency generation spectrometer has been described previously.[62-64] Briefly, spectra were collected using either the *ssp*, *ppp*, or *sps* polarization combination, corresponding to *s*-or *p*-polarized sum frequency, visible, and infrared beams, respectively. The *ssp* combination probes vibrational modes having transition dipole moment components aligned perpendicular to the interface, the *sps* polarization combination is sensitive to components of the

vibrational modes that are oriented parallel to the interface, and off-diagonal elements of the nonlinear susceptibility tensor are probed in the *ppp* polarization .[64]

The incident IR beam and visible beam overlap spatially and temporally in an external geometry at the air:squalene interface. SFG spectra were taken with *ssp, ppp, and sps* polarization combinations, of which the three letters stand for the polarizations of the output SFG beam, the incident visible beam, and the incident IR beam, respectively. Among them, *ssp* and *sps* polarization combination probe the components of the vibrational modes that are oriented normal and parallel to the surface, respectively. The ambient temperature and relative humidity in the laboratory were maintained at 20 ± 1 ºC and 30 – 50%. All measurements were carried out in duplicate. It takes about 45 minutes to collect one SFG spectrum over the 2600-3100 cm^{-1} range, including collection of the background (IR beam blocked), to obtain SFG spectra at the quality reported in this study.

2.2.4 Optical Profilometry

Optical microscopy samples were prepared using the same technique described in Section 2.2.1. The thickness of the spin-coated squalene film was characterized using a 3D optical microscope (Bruker ContourGT, 130 nm lateral and better than 1 nm height resolution). We prefer this approach over atomic force microscopy, which produces noise due to material accumulation on the tip during scans.[65] A portion of the fused silica substrate was covered with Kapton tape so as to provide an internal zero-height reference (RMS roughness of 9 to 10 nm, determined for several 300 x 300 μm^2 areas). On the atomic scale, the RMS roughness of the uncoated fused silica substrates is 0.4 nm, as determined by atomic force microscopy (AFM) from several ten-μm linescans.[66]

2.3 Results and Discussion

2.3.1 SFG Analysis of the Surface of a Squalene Film

A representative *ssp*-polarized spectrum of the surface of a squalene film in the C–H and O–H stretching regions (2600 – 3800 cm^{-1}) is shown in Figure 2.1. Because the spectrum is normalized to the reference nonresonant signal from gold and the signal from it is relatively low towards the edges of the spectrum due to weak IR power there, the signal-to-noise ratio is relatively low on both ends.

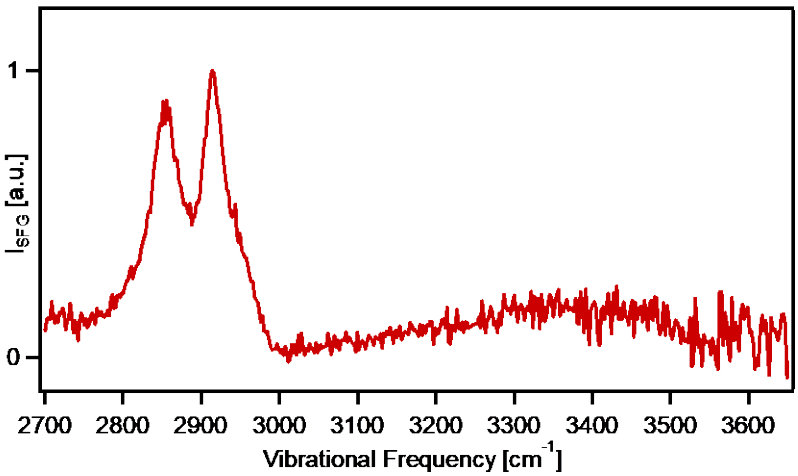

Figure 2.1: A representative ssp-polarized vibrational SFG spectrum of the surface of a squalene film.

Considering the molecular structure of squalene, the most striking feature of the spectrum shown in Figure 2.1 is the lack of a distinguishable signal around 3050 cm^{-1}, which would be expected for the vinylic (=C–H) modes, despite the fact that squalene contains six vinylic C–H bonds.[59, 67-69] The other polarization combinations we used did not show signal intensity in that frequency region (Figure 2.2). This finding indicates that the vinylic C–H bonds are oriented such that their transition dipole moments sum to zero, which would be expected for all *trans*-configured modes, or modes that are symmetrically distributed in and/or normal to the x-y plane of the interface. Next, the O–H stretching region appears to contain a weak broad band, indicating the presence of some water molecules at the squalene surface at ambient relative humidity. The 3400 cm^{-1} center frequency of this

broad band matches that of bulk liquid water, indicating perhaps the presence of a loosely hydrogen-bonded network of water molecules.[70]

The sp^3-hybridized C–H stretching region (below 3000 cm^{-1}) is dominated by two main peaks at around 2855 cm^{-1} and 2915 cm^{-1}, which are usually assigned as methylene symmetric and asymmetric stretches, respectively.[57, 59, 71] A shoulder appears near 2965 cm^{-1}, which is normally attributed to methyl asymmetric stretches[72-73] or methyl Fermi resonances.[74] The considerable SFG intensity at 2900 cm^{-1} indicates the presence of additional modes, given the spectral resolution of our instrument (~8 cm^{-1} near 2900 cm^{-1}). Indeed, all-trans-configured n-octadecyl silane show no signal intensity in this frequency region.[75]

While the frequencies of the two dominant peaks and the shoulder are consistent with reported IR spectra of squalene in literature,[76-77] the published spectral assignments have only been approximate in the C-H stretching region. This lack of information is not surprising, given the complexity of squalene's molecular structure.

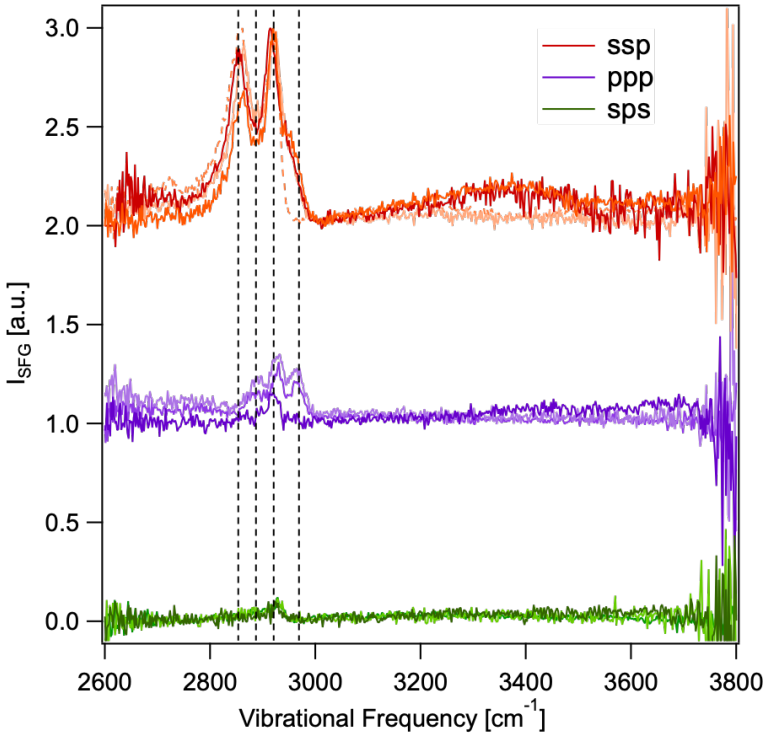

Figure 2.2: Replicates of ssp-, ppp-, and sps-polarized SFG spectra of the surface of squalene films on fused silica.

Replicates of *ssp*-, *ppp*-, and *sps*-polarized SFG spectra of the surface of squalene films on fused silica collected are shown in Figure 2.2. The spectra were all normalized to the highest peak in *ssp*-polarized spectra to demonstrate the relative intensity of different polarization combinations. The *ssp*-polarized spectra show the highest signal-to-noise ratio and the *sps*-polarized spectra have very low spectral intensity. The low intensity of *sps*-polarized spectra can be explained by the nearly isotropic orientation of functional groups azimuthally within the x-y plane.

These spectra were collected from different samples prepared on different days and the spectral features are generally consistent. The C–H stretching region in the *ssp*-polarized spectra is dominated by two main peaks at around 2855 cm^{-1} and 2915 cm^{-1} and a shoulder around 2965 cm^{-1}. One of the *ssp*-polarized spectra is an outlier without the shoulder band and is notated with dashed lines. The *ppp*-polarized spectra generally exhibit three peaks at around 2965 cm^{-1}, 2930 cm^{-1}, and 2900

cm^{-1} and the *sps*-polarized spectra only contain a small bump at around 2930 cm^{-1}. The broad O–H stretching band only appears to be significant in some *ssp*-polarized spectra.

2.3.2 Optical Profilometry Reveals Non-Uniform Height vs. Distance Profiles with 100 nm to >1 mm Tall Features.

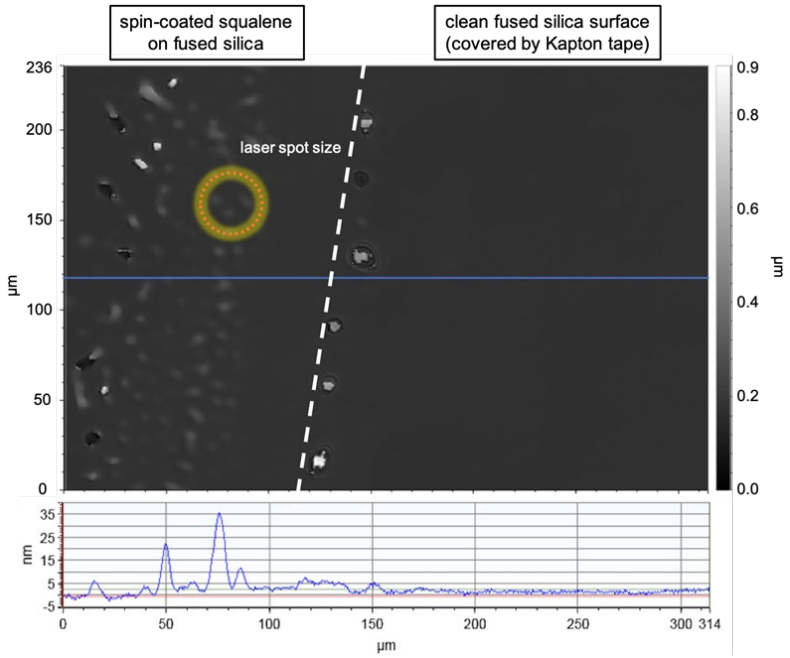

Figure 2.3: *Top panel:* A 3D optical image of the border of spin-coated squalene on fused silica (on the left) and the clean fused silica surface (on the right). The size of a laser spot is indicated with the orange circle. *Bottom panel:* The height profile of the blue line across the field of view.

We have examined the spin-coated film with 3D optical microscopy (Bruker ContourGT). The 3D optical microscopy shows scattered droplet-like patches of squalene, shown in Figure 2.3. The height of the droplets ranges from ~20 nm to ~200 nm (the spots with sharp edges and higher heights are likely to be dust). We have also attempted using AFM (Bruker Dimension FastScan) to characterize the film surface. However, because squalene is oily and sticky, we found that it would accumulate on the tip during scans and introduce noise to the image. Optical profilometry circumvents this problem as it is a non-contact method.

2.4 Implications for Chemistry of the Indoor Environment and Conclusions.

The approach presented here has already shed light on different aspects of the interfacial structure and reactivity of squalene. Further elucidation of the surface properties of squalene was made possible through collaboration with Dr. Michael von Domaros in the Tobias group at UC Irvine. With 50 vibrational normal modes in the C–H stretching region and close to 125000 possible conformations stemming solely from the dihedral flexibility of the main carbon chain, squalene is a spectroscopically complex molecule.

We began to disentangle this complexity with MD simulations that revealed strong orientational/conformational preferences of interfacial squalene molecules. Our approach indicated that the vinylic =C–H oscillators point up and down in the interfacial region, largely resulting in an unanticipated cancellation of the SFG signal intensity at the expected oscillator frequency of ~3050 cm^{-1}. Vibrational peak assignments derived from common, long alkyl chain-containing molecules, which would attribute the 2855 cm^{-1} and 2915 cm^{-1} peaks to methylene stretches, were found to be at variance with the largely *anti*-configured CH_2 groups dominating the interfacial squalene molecules in the MD simulations. Instead, the spectral features at these frequencies are likely to be largely due to the methyl groups that are oriented along the surface normal. Next steps require the synthesis of isotopologues (^2H or ^{13}C) in pure and homogeneous form to separate the SFG signal contributions from different vibrational modes.[78-80]

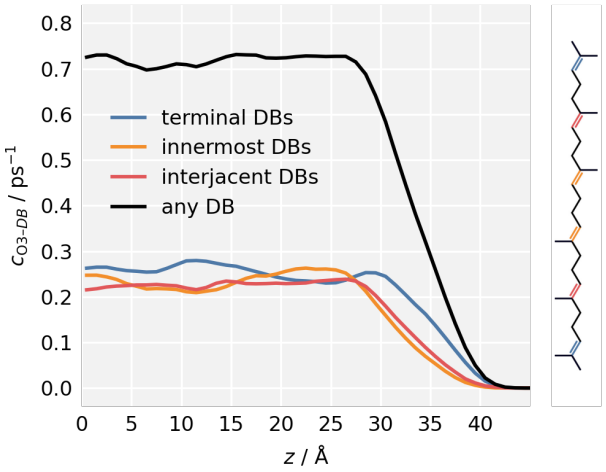

Figure 2.4: Position-dependent ozone–double-bond collision rates, $c_{O3\text{-}DB}$.

Another key finding of this study is that the concentrations of various types of squalene double bonds are predicted to differ in the interfacial region compared to the bulk. This prediction has direct implications for the reactivity of squalene with ozone and other indoor air oxidants. While ozone does not show any preference to collide with a particular class of double bonds in the bulk, collisions with terminal double bonds are more frequent than others in the interface (Figure 2.7). Collision rates between ozone and terminal double bonds were estimated to be higher in the interface when compared to those with interior bonds. This outcome warrants a more detailed investigation in kinetic models describing this important aspect of indoor air chemistry, as it would point towards a reaction mechanism in which the differing accessibility of each of the six C=C double bonds to ozone would determine which oxygenated gas phase product would be formed. As relative humidity values indoors can vary considerably during the day, the role of adsorbed water, clearly observed in the SFG spectrum shown in Figure 2.1, should also be investigated, especially given recent results indicating an intricate connection between viscosity and water:squalene interactions in reverse micelles.[81] Similar to what has been reported for secondary organic material formed from the atmospheric oxidation of plant-derived terpenes,[82-83] water activity-dependent viscosity may act as a "gate" to permit or deny incoming

oxidants like ozone access to C=C double bonds in the bulk of squalene. Such an effect would then result in the production of volatile organic compounds and possible lung irritants from the C=C double bonds in the nanometer-thin surface region described here under conditions of low relative humidity (typically daytime). At high relative humidity (typically nighttime), more volatile organic compounds could be formed from C=C double bonds inside the bulk organic film. This effect, if it exists, would be counterbalanced, however, by the diurnal variation of indoor ozone concentrations.

Chapter 3:

Skin Oil and Squalene Ozonolysis

Portions of this chapter appear in the following publications:

Butman, J. L.; Thomson, R. J.; Geiger, F. M., Unanticipated Hydrophobicity Increases of Squalene and Human Skin Oil Films Upon Ozone Exposure. *J Phys Chem B* **2022**, *126* (45), 9417-9423

3.1 Introduction

Having characterized squalene-ozone interactions using a combination of spectroscopy and modeling, we were interested in further investigating surface chemical transformations due to common indoor heterogeneous reactions. As the outcomes described in Section 2.4 revealed, we found similarities between this transformation and previously known atmospheric aerosol surface characteristics. We wanted to develop an experiment that would allow us to see the effect of changing relative humidity, kinetic factors, and controlled ozone levels.

Depending on the relative humidity (RH), ozonolysis may be limited to the surface region of the deposited skin oil layers and films or involve bulk-localized C=C double bonds. The surface structure and chemistry may thus be subject to humidity-dependent "gating", similar to what we previously reported for secondary organic aerosol material relevant for atmospheric chemistry outdoors.[82] Yet, despite the importance of heterogeneous processes in indoor chemistry, surface-selective studies of C=C double bond oxidation relevant to indoor environments are sparse.[84] Laboratory experiments tracking heterogeneous ozonolysis are complicated by the large bulk response to spectroscopic readouts, or require off-line analysis.[26, 85-86] Bringing these approaches indoors to probe real, complex interfaces under indoor relevant conditions of atmospheric pressure, room temperature, 30-50% RH and 10-50ppb of O_3 holds the promise of aiding in our molecular understanding of indoor heterogeneous chemistry.[87-88]

The ozonolysis of squalene and the evolution of its products as depicted in Figure 1.2 has been studied extensively with bulk analytical methods like MS.[42, 44, 46, 89-92] A lack of on-line surface analysis that is distinguished from the bulk response is what prompted our investigation into surface ozonolysis of skin oil and its components. We hypothesized that surface specific characterization for these transformations is critical for a complete understanding of indoor sVOC evolution. By

conducting on-line SFG analysis we would be able to obtain molecular information about squalene and skin oil ozonolysis that was both surface selective and bond specific.

3.2 Methods

3.2.1 Integrated SFG Spectroscopy Gas Flow Setup

We employed a home-built flow cell machined from PVC described previously.[93-94] The fused silica optical windows, Swagelok inlet fittings, Viton O-rings, and the flow cell were rinsed with methanol (Fisher Scientific, HPLC grade) and Millipore water alternately and dried with nitrogen gas. The Swagelok fittings were dried in a 160 °C oven for 1 hour. The windows, block, and O-rings were then plasma-cleaned for 10 minutes (Harrick Plasma, 18W, set on "high") immediately prior to starting an experiment. Following this cleaning process, the silica windows gave no SFG signal in the C-H stretching region over 45 minutes of spectral data acquisition time.

The multi-path flow system used here was adapted from the setup used in our previous work.[93-94] Briefly, a stream of helium gas (Ultra-High Purity Grade, 99.999%) was split into a "dry" path, through which it directly reached the sample stage, and a "wet" path, wherein it passed through a bubbler containing Millipore water in order to control the RH of the reaction being monitored. Ozone was generated by passing a stream of oxygen diluted in helium through an ozone generator (Teledyne, Model 430). Use of a bypass loop and appropriately placed on-off valves allowed for rapid ozone rise times when starting ozone exposure in the sample cell.

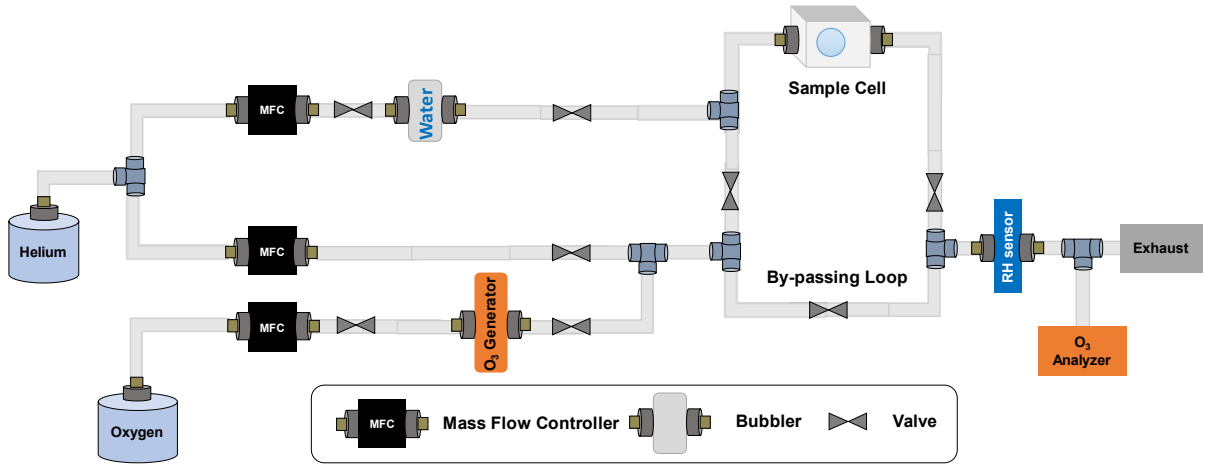

Figure 3.1: Integrated SFG gas-flow setup

Ozone concentrations were monitored during the experiments using an ozone detector (Teledyne API Model 430) and kept to a range of 10-50 ppb to be representative of ozone concentrations that have been both reported in actual indoor environments as well as model chambers.[38, 86, 95-96] Flow rates were controlled and monitored by digital mass flow controllers (MFCs, Alicat) for each path and are reported in standard liters min^{-1} (SLPM). All experiments were conducted at an ambient laboratory temperature maintained at 22.0 (±0.5) °C. Skin oil samples were obtained from one human who did not use personal care products on the day of sampling. Following the method published by the Abbatt group,[52] the subject swiped their thumb over their forehead once and deposited the collected skin oil onto a fused silica window, smearing the oil to create a thin film.

3.2.2 Contact Angle Goniometry

Contact angle goniometry is an effective approach for measuring surface hydrophobicity.[97-98] Sessile contact angles were measured using a computer-interfaced First Ten Ångstroms goniometer (FTÅ 125). Ultrapure water (Milli Q, Millipore Inc., 18.2 MΩ cm) in a syringe was used to create a droplet of water less than 3 mm in diameter on the substrate under investigation. Static contact angles were determined from on-the-fly analysis of images collected at 1 Hz frame rate over a 40 second

acquisition period starting at t=0. Samples used for contact angle measurements were not used for subsequent contact angle or spectroscopic measurements. Each substrate has a surface area large enough to accommodate 4-6 droplets, whose contact angles they made with the substrate were subsequently averaged to give the final point estimate and standard deviation of the contact angle measurement. For each experimental condition of pre- and post-ozone exposure, at least three windows were studied, for a total of 12 to at least 18 measurements per condition.

To further characterize surface properties post-ozone exposure, we employed contact angle goniometry. The measurement provides an indication of how hydrophobic (high contact angles) or hydrophilic (low contact angles) the surface of a material is. While we expected the contact angles to decrease upon ozonolysis relative to the starting condition (no ozone) due to polar carbonyl-containing functional groups remaining with the film material as shown in Figure 3.8, we observed significantly larger contact angles following exposure to 10-50 ppb of ozone in 40% relative humidity for 20 minutes. This exposure sequence is the same we employed in the SFG experiments summarized in Figure 3.4.

Longer observation of the contact angles reveals a continuous lowering of the contact angle, which is attributed to the sessile drop flattening as capillary action causes the water to spread on the surface.[99-100] Nevertheless, the result seems to indicate interesting dynamics when ozone-processed surface films are wetted in indoor settings, such as kitchens and bathrooms.

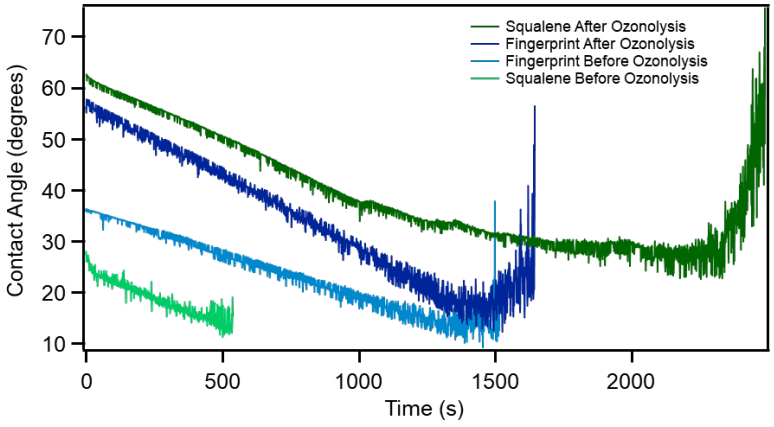

Figure 3.2: Extended contact angle analysis. The time axis reflects the time during which the sample contains the water drop needed to determine the contact angle.

3.3 Results and Discussion

3.3.1 Skin Oil SFG Spectra Are Highly Reproducible

In preliminary studies evaluating the viability of skin oil as a representative analyte for SFG analysis, skin oil from three different subjects were collected using the same procedure described in Section 3.2.1.

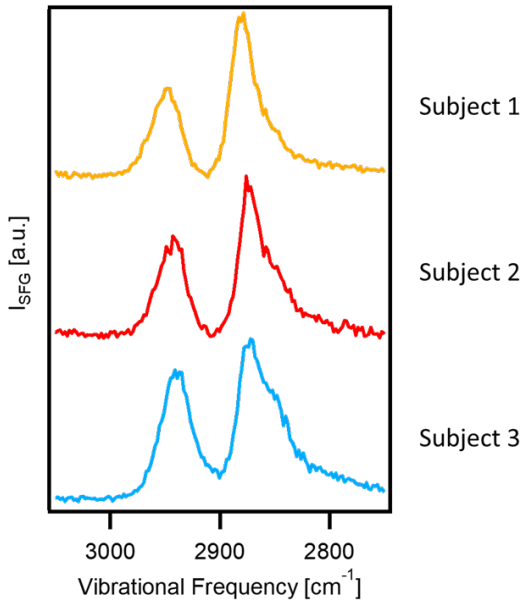

Figure 3.3: *ssp*-Polarized SFG spectra of skin oil from three different human subjects. Subject 1 provided skin oil for all other experiments in this study.

3.3.2 SFG Spectra Show Loss of C-H Oscillators Upon Ozonolysis

Figure 3.4 shows the *ssp*-polarized SFG spectra of squalene spin coated on a fused silica window and of human skin oil deposited on a different fused silica window before and after exposure to 10-50 ppb of ozone, both recorded at 40% relative humidity. Neither spectrum shows resonances above 3000 cm^{-1}, typically associated with vinylic =C-H stretches.[59, 67, 101-102] Our earlier work on squalene showed that the vinylic =C-H stretches are absent due to symmetry, orientation, and weak IR cross sections that diminish their SFG responses.[65]

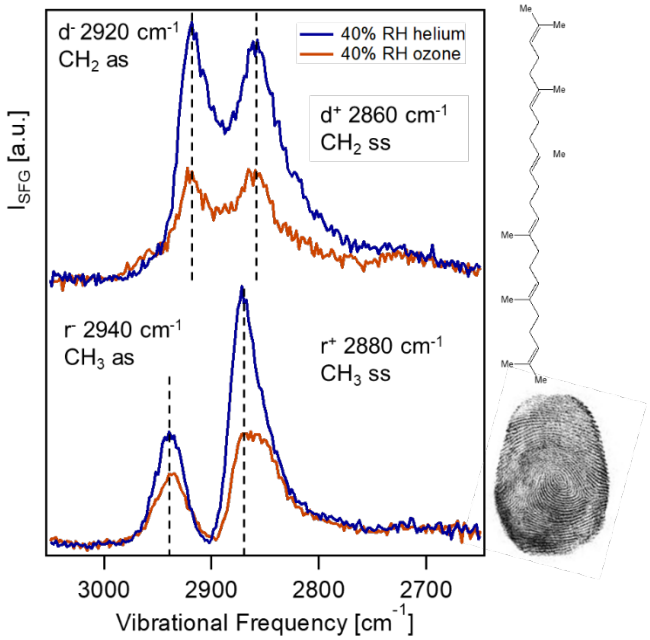

Figure 3.4: *ssp*-Polarized SFG spectra of squalene (top) and skin oil (bottom) before (blue) and after (orange) 20 minutes of exposure to 10-50ppb of ozone at 40% RH. Measurement performed at 1 ATM total pressure and at room temperature. Fingerprint image from public domain.

The spectra reveal clear differences between the squalene and skin oil sample. The skin oil sample produces two modes in the SFG spectrum that are centered at 2940 and 2880 cm^{-1}, with negligible signal intensity at 2900 cm^{-1}, while the spectral line shape obtained from the squalene spectrum is characterized by two peaks at 2920 and 2860 cm^{-1} and considerable signal intensity at 2900 cm^{-1}. Spectra recorded with other polarization combinations, shown in Figure 2.2, are less intense, and

don't show any features above 3000 cm^{-1}, either. Atomistic simulations indicate the second-order vibrational spectrum of squalene is dominated by its methyl groups pointing with their C_{3v} symmetry axis along the surface normal, while the six olefinic C-H groups are oriented to cancel one another out per symmetry, as explained in Section 2.4.[65] As skin oil is a complex mixture containing many lipids, including some squalene, we do not provide a spectroscopic assignment of the 2940 and 2880 cm^{-1} modes in the skin oil SFG spectra at this time. Yet, these frequencies are associated with the methyl group asymmetric and symmetric stretching modes, at least based on literature precedent of common aliphatic compounds.[65, 72-74] Despite the chemical complexity of skin oil, its SFG spectra are highly reproducible over a total of multiple skin oil samples taken over the course of several months (Figure 3.3) indicating perhaps a certain number of surfactants dominate the surface structure irrespective of naturally varying chemical composition in the bulk.

Figure 3.4 shows that exposure to several tens of ppb of ozone at 40% relative humidity leads to considerable reductions in the SFG signal intensity of both the squalene and the skin oil samples. While the intensities of the two prominent modes from the squalene sample diminish rather equally, the intensity loss in the skin oil spectrum appears to involve largely the 2940 and 2880 cm^{-1} modes, with significant signal intensity remaining at 2850 cm^{-1}, the characteristic mode of CH_2 symmetric stretches of aliphatic compounds.[57, 59, 71] Taken together, the spectra indicate a loss of SFG signal intensity at frequencies associated with methyl groups, which is consistent with the formation of CH_3-containing volatile organic compounds like acetone, as indicated in Figure 1.2. The material remaining on the substrate would then consist of molecules having their share of methylene groups enriched relative to that of the methyl groups. The observation that some spectral intensity is present after ozonolysis indicates that the reaction has evidently self-terminated before all film material was consumed.

3.3.3 Contact Angle Measurements Show Increased Hydrophobicity Following Ozonolysis.

To further characterize surface properties post-ozone exposure, we employed contact angle goniometry (Figure 3.5). The measurement provides an indication of how hydrophobic (high contact angles) or hydrophilic (low contact angles) the surface of a material is. While we expected the contact angles to decrease upon ozonolysis relative to the starting condition (no ozone) due to polar carbonyl-containing functional groups remaining with the film material (Figure 3.8), we observed significantly larger contact angles following exposure to 10-50 ppb of ozone in 40% relative humidity for 20 minutes.

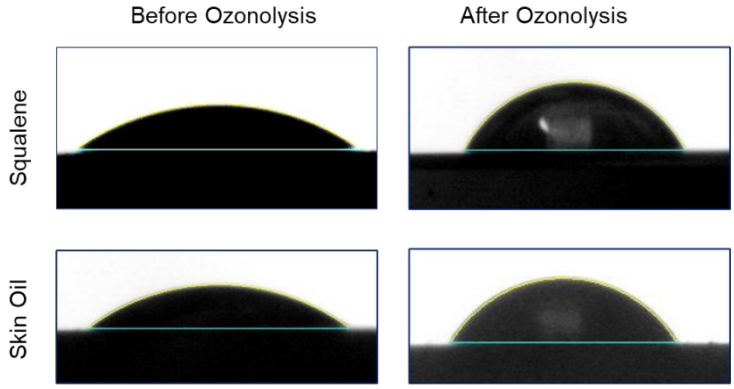

Figure 3.5: Contact angle images and average contact angles with standard deviation measured before (left) and after 20 minutes of exposure to 10-50 ppb of ozone at a constant relative humidity of 40% (right).

Substrate	Contact angle before ozonolysis (std. dev.)°	Contact angle after ozonolysis (std. dev.)°
Plasma-cleaned silica	3(1)	-
Squalene	35(4)	55(9)
Skin Oil	30(4)	58(6)

Table 3: Contact angles before and after ozonolysis at 40% relative humidity.

3.3.4 Optical Profilometry Shows no Major Morphology Changes Due to Ozonolysis

Optical profilometry was used to rule out morphology changes on the scale of a few tens of nanometers to 300 microns as the cause of increased hydrophobicity following exposure to ozone. The root mean square roughness (Sq) of the skin oil surfaces was measured before and after ozonolysis at 30% RH. Roughness measurements were made in 4 different regions (300 μm × 300 μm) on the surface of a given sample. A total of 3 different samples were analyzed for a grand total of 24 different pre- and 24 post-ozonolysis conditions using an optical profilometer (Bruker Contour GT) that generated 3D images of the surfaces that were analyzed with Profilm3D.

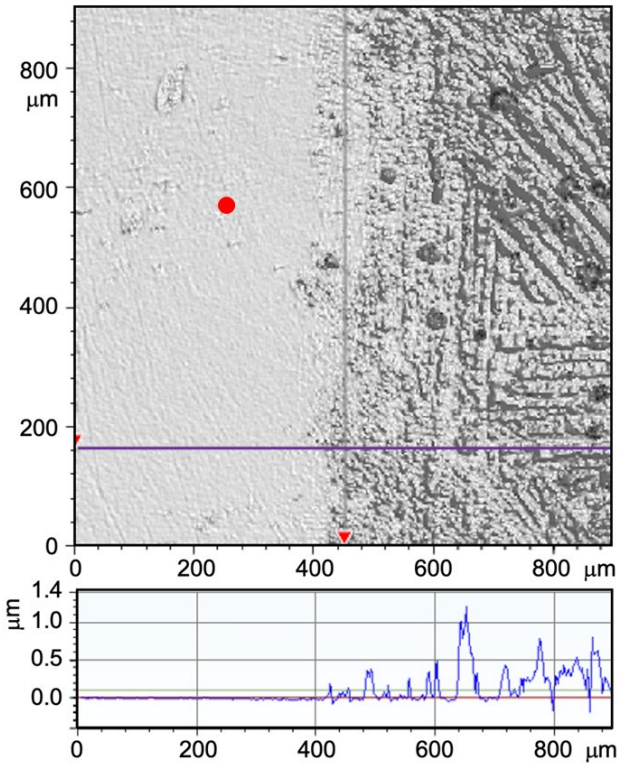

Figure 3.6: Optical profilometry image and horizontal height profile of a wiped fingerprint on a silica window. Red circle indicates SFG laser spot size.

Sample	*Sq Before (μm) (std. dev.)*	*Sq After (μm) (std. dev.)*	*Percent Change in Sq*
1	0.16 (0.03)	0.15 (0.03)	-3.51 (0.08)
2	0.13 (0.04)	0.16 (0.05)	23.9 (0.10)
3	0.15 (0.05)	0.14 (0.05)	-3.22 (0.11)
4	0.25 (0.07)	0.26 (0.08)	6.94 (0.16)
5	0.26 (0.05)	0.26 (0.07)	1.01 (0.13)
6	0.28 (0.06)	0.27 (0.08)	-0.97 (0.16)
7	0.42 (0.10)	0.35 (0.04)	-16.7 (0.14)
8	0.12 (0.03)	0.14 (0.07)	23.1 (0.13)
Average	0.22 (0.16)	0.22 (0.17)	3.82 (0.37)

Table 4: The root mean square roughness (Sq) of select skin oil surfaces measured before and after ozonolysis.

3.3.5 Kinetic Ozonolysis Observed by SFG of Skin Oil and Squalene

With the flow setup and the capabilities of the laser system described in Section 3.2.1, we have started to investigate the ozonolysis process of squalene and skin oil, as shown in Figure 3.7.

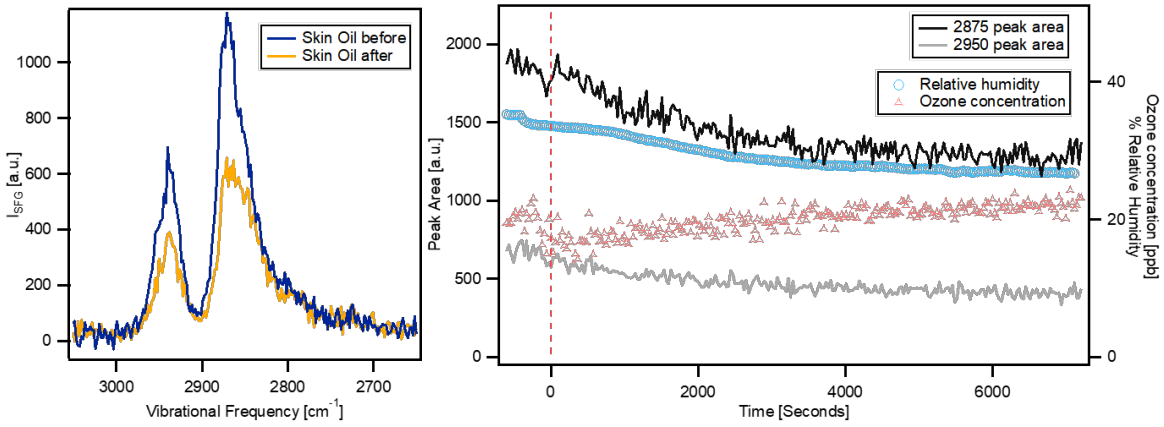

Figure 3.7: (left) Representative ssp-polarized SFG spectra (left) of skin oil before (in blue) and after (in orange) ozone flow. (right) During all experiments, RH (light blue) was maintained at 20-40%. Ozone concentration (light red) was maintained at 10-50ppb. The vertical dashed red line at t=0 represents when the bypass line was redirected from the exhaust to the sample cell, beginning ozonolysis of the skin oil film. The black and gray traces represent the integrated area underneath the peak at 2875 cm^{-1} and 2950 cm^{-1}, respectively.

The SFG results reflect the conditions described in Section 3.3.2 linking C-H oscillator loss due to ozonolysis with the overall decrease in SFG signal intensity. This loss appears to slow or stop entirely at around t=4000s, suggesting that by then the surface skin oil-ozone reaction at standard indoor relative humidity and ozone concentration is mostly complete. Further investigation towards

tracking the ozonolysis of squalene and skin oil on a variety of indoor-relevant surfaces in real time and under indoor relevant conditions such as ambient pressure, temperature, varying relative humidity, and varying ozone concentrations is needed.

3.4 Implications for Chemistry of the Indoor Environment and Conclusions

The results shown in Figure 3.5 indicate that exposing squalene and skin oil samples to ozone under our stated experimental conditions produces a more hydrophobic material relative to pre-O_3 exposure. We previously reported on the phenomenon of increased hydrophobicity after the ozonolysis of an alkene tethered to fused silica using silane chemistry, employed as a highly idealized model system for atmospheric organic aerosol particles.[102] We were surprised to find sequences of sample exposure to water vapor and ozone that are common indoors to yield similar outcomes on the more complex materials studied here.

To provide a rationale for the origin of the increased hydrophobicity, we considered several scenarios: first, the polar functional groups formed during ozonolysis should point away from the air (which is the least polar environment in this system) and into the processed bulk film, as pictured in Figure 3.8. This scenario would not make a difference in terms of a change in polarity as the films' surface would consist of their hydrophobic moieties both before and after reaction with ozone. Nevertheless, the larger contact angles are certainly consistent with the notion that the polar functional groups formed point away from the aqueous droplet, into the films' interiors.

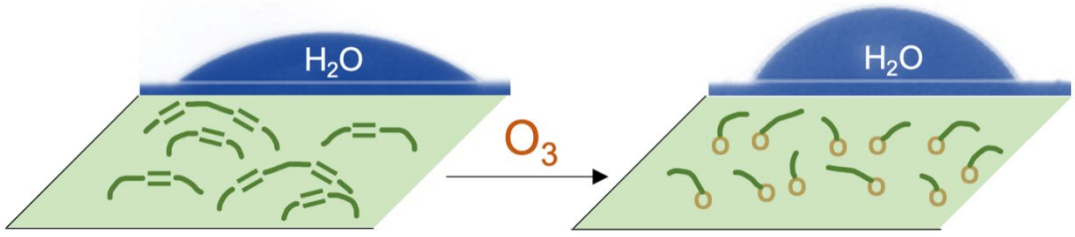

Figure 3.8: Cartoon of C=C double bond loss during ozonolysis and polar oxygenated functional group orientation into the film's interior and associated increase in hydrophobicity.

We then considered changes to film morphology, which was motivated by an earlier publication on the formation of organic aggregates having heights of 100s of nanometers and even microns from the ozonolysis of self-assembled alkene monolayers observed by the Finlayson-Pitts group using AFM, albeit at considerably higher ozone concentrations (1 ppm).[103] Unfortunately, as we had showed earlier,[65] AFM probes become coated with the soft matter that constitutes the (several hundred nm thick) squalene and skin oil films studied in our present work so that the images become noisy, and the 3D optical microscope proved to be informative. We used this method to determine the root mean square roughness (Sq) of the skin oil surfaces before and after ozonolysis using Profilm3D online software.[104] A total of 64 roughness measurements were made in 4 different regions (300 μm × 300 μm) on eight films before and after ozone exposure (Table 2). Our detailed analysis showed the Sq value differences pre- and post-ozone exposure to be statistically insignificant (220 ± 160 nm vs 220 ± 170 nm for all eight samples, four regions per sample, pre and post ozone; please note that the average of the standard deviation in Sq for each of the eight samples is 50 nm; standard error propagation was used for the standard deviation of all the eight samples. Recall that the Sq estimates for the bare silica substrate is around 10 nm from optical profilometry and 0.4 nm from AFM). We conclude that film roughness changes are not discernable, at least for the conditions of our experiments, and if they occur, they are not on the order of magnitude reported in the self-assembled monolayer work.[103]

At first glance, these results appear to be at variance with previous interesting infrared spectroscopy studies from the Liu group, which reported an increase in bulk water uptake following ozonolysis of squalene films.[45] However, that study probed predominantly water in the bulk material of the sample. The surface selectivity of SFG spectroscopy, along with the contact angle measurements now allow us to posit that our samples are likely terminated by a hydrophobic shell,

while there may indeed be water molecules present in the bulk below. Prior mass spectrometric studies of squalene ozonolysis have shown that an increase in water vapor concentration increases Criegee intermediate formation and gas-phase VOC product concentrations by a factor of 3.[46]

We then considered recent work by the Bertram group, who reported liquid squalene and skin oil exposed to ozone form a new condensed phase comprised of oligomeric ozonolysis products.[105] These higher molecular weight oligomers could show increased hydrophobicity compared to unreacted squalene and skin oil, but the optical microscopy data reported by the Bertram group indicate them to be inside of the imaged sample drops. These observed oligomeric phases also evolve over a much greater timescale than we observed, on the order of hours rather than minutes, and with higher concentrations of ozone at lower RH%. If such a new phase formed inside the films studied in our present work, it would likely be inaccessible to the water drops used in our sessile contact angle measurements.

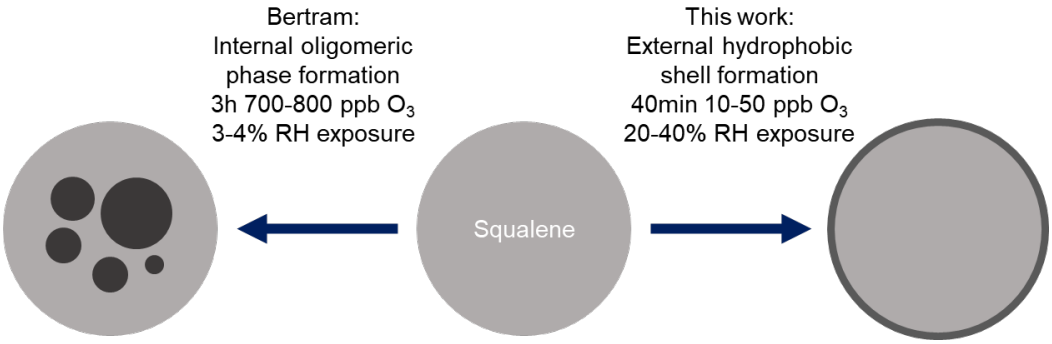

Figure 3.9: Illustration of the difference of observed phase formation in squalene.

Given our data and the prior work discussed here, the increased hydrophobicity we observe following ozonolysis is unlikely to be due to sole reorientation of newly installed polar functional groups, morphological changes, or the formation of a new phase. However, our findings are consistent with lower octanol-water partition coefficients (logP) for alkenes vs alkanes.[106] Indeed, C5 to C8 hydrocarbons exhibit logP values that are about 0.5 to one log unit lower when double bonds are

present, as in, for instance, n-pentane (logP=3.45) vs 1,4-pentadiene (2.48); n-hexane (4.00) vs 1-hexene (3.40) vs 1,5-hexadiene (2.80); n-heptane (4.50) vs 1-heptene (3.99); n-octane (5.15) vs 1-octene (4.57). This outcome is attributable to the polarizable π-electron system of the C=C double bond, with which water can form hydrogen bonds ("πH bonding")[107] having dissociation energies that range from modest (10 kJ mol^{-1} for ethene or 1,3-butadiene) to reasonable strong (20 kJ mol^{-1} 2-methyl-2-butene and 27 kJ mol^{-1} for 2,3-dimethyl-2-butene).[108] The loss of the polarizable C=C double bonds due to ozonolysis is consistent with the observation of increased hydrophobicity of the films we investigated here.

Chapter 4:

Indoor Air and Oil Mixing

4.1 Introduction

As stated previously, skin oil is a multicomponent system comprised of triacyl glycerols (~25%), unesterified fatty acids (~25%), wax esters (~22%), squalene (~10%), mono- and diacyl glycerols (~10%), and lesser amounts of sterol esters, sterols, phospholipids, and other species.[109] While we have been able to elucidate many aspects of squalene-air transformations including orientation to the surface when interacting with ozone,[110] and loss of C-H oscillators therein leading to hydrophobicity,[98] squalene constitutes only one component of skin oil. The difference observed between squalene and skin oil SFG spectra in Chapter 2 indicates that the surface characteristics of the skin oil system cannot be modeled solely on the behavior of squalene.

Oleic acid is another commonly studied component of skin oil, also used as a model system much like we have used squalene.[36, 111] Zahardis et al. studied the ozonolysis of particles containing mixtures of oleic acid with amines, reporting high retention of unoxidized oleic acid even at high O_3 concentrations, suggesting O_3 diffusion into the particle core had been disrupted by the formation of a semi solid crust.[112]A kinetic multilayer model developed by Pfrang et al. simulated the ozonolysis of particles containing mixed organic components including oleic acid.[113] They illustrated that the formation of a crust at the particle surface could explain previous measurements of chemical loss rates in oleic acid-containing particles by acting as a diffusion barrier. In addition, Milsom et al. studied the reaction between O_3 and particles containing mixtures of oleic acid and sodium oleate and presented experimental evidence of an inert surface crust forming during ozonolysis. Considering the effect that phase separation could have on ozone penetration rates, the surface-partitioning behavior of the components of skin oil is important to understanding the skin oil-ozonolysis reaction indoors. When a gas-phase ozone molecule approaches surface-deposited skin oil indoors, it must collide with a C=C double bond to cleave it. In Section 2.4, we were able to elucidate from experimental and modeling

studies that ozone would prefer to collide with one of the outermost C=C double bonds of squalene at the surface.

If, for example, squalene favored partitioning underneath other skin oil components like oleic acid, ozone molecules would have to 'burrow' through layers of other skin oil components to reach the reactive subspecies underneath. Importantly for our purposes, oleic acid gives SFG signal that is qualitatively distinct from squalene, which allows us to distinguish between oleic acid and squalene surface signal. In preparation for potential ozonolysis studies on a squalene-oleic acid binary mixture, we wanted to investigate surface partitioning properties and phase separation mechanics of this binary system. Squalene is normally below 20% of total skin oil composition, so we also tested whether there was a mixing hole at which a binary squalene/oleic acid mixture in this range might become a heterogeneous, phase separated solution.

4.2 Methods

4.2.1 Materials

Samples were prepared by dissolving squalene (Sigma-Aldrich, Part No. S3626, >98%, used as received) and oleic acid (Sigma-Aldrich, Part No. O1008, >99%, used as received) in deuterated chloroform, $CDCl_3$ (Sigma-Aldrich, Part No. 151823, 99.8 atom % D), and spin-coating at 3000 rpm onto either a fused silica optical window substrate (ISP Optics, Part No. QI-W-25-3) or CaF_2 window (ISP Optics, Part No. CF-W-25-3) that had been sonicated in methanol (Fisher Scientific, Part No. A452-4, HPLC grade), rinsed with methanol and Millipore water alternately, and then plasma cleaned. The coated sample window was clamped vertically on a translational stage. The ambient temperature and relative humidity in the laboratory were maintained at 20 ± 1 ºC and 30 – 50%, respectively.

4.2.2 SFG Spectroscopy of Squalene and Oleic Acid Mixtures

Our preliminary squalene and oleic acid mixing studies focused on a thorough exploration of squalene and oleic acid SFG signals in various polarizations and reflection geometries. Because a fluorescent baseline color center overlapping with the C-H stretching signal is produced when the upconverter laser beam passes through silica in internal reflection mode, preliminary SFG studies on this mixture were carried out on CaF_2. Samples of squalene, oleic acid, and a binary mixture of the two in equal molar ratios were prepared as described in Section 4.2.1 and observed using both *ssp*- and *ppp*-polarized SFG, in both internal and external reflection geometries. Based on our observations from this experiment, we focused on comparing the *ssp*-polarized SFG spectra of squalene and oleic acid mixtures. As we focused on external reflection, we returned to using silica windows which acts as a window glass analog as covered in previous chapters.

4.2.4 Scattering Studies of Squalene and Oleic Acid

We built a simple light scattering setup to determine whether a mixing hole exists for squalene and oleic acid mixtures (Figure 4.3). Briefly, a 405nm laser (Micro Laser Systems, Model L4405N-7-TE) was passed through a 1.5 microliter sample cuvette (Fisher Scientific, 14-955-127). The scattered laser light 90° from the incident beam was focused into a spectrometer (Ocean Optics, USB4000) and the scattered intensity was recorded.

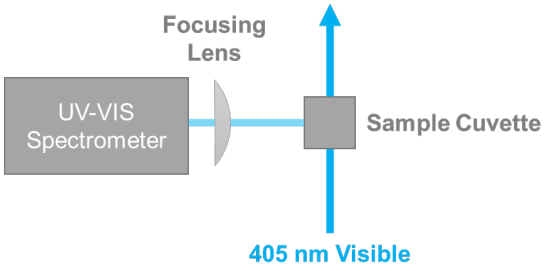

Figure 4.1: Simple diagram of the scattering setup. Most of the incident 405 nm laser light transmitted through the sample cuvette. Observed scattered light was focused into the spectrometer at 90° from the incident beam.

4.3 Results and Discussion

4.3.1 Oleic Acid Dominates Squalene SFG signal at the Air-Oil Interface

As shown in Figure 4.1, *ssp*-polarized SFG signal of oleic acid at the external air interface (top right) has three characteristic major peaks in the C-H stretching region. Qualitatively, oleic acid dominates the observed external spectra of the binary 1:1 mixture on CaF_2. The internal reflection spectra (bottom) of squalene and oleic acid are more alike, suggesting that their vibrational modes are similarly oriented on the internal CaF_2 interface. In the 1:1 mixture, oleic acid's characteristic 3 spectral peaks occurring at 2850 cm^{-1}, 2935 cm^{-1}, and 2900 cm^{-1} are clearly visible in the external geometry. While squalene is equally present in the mixture on a molar basis, the spectral line trace predominantly displays oleic acid character.

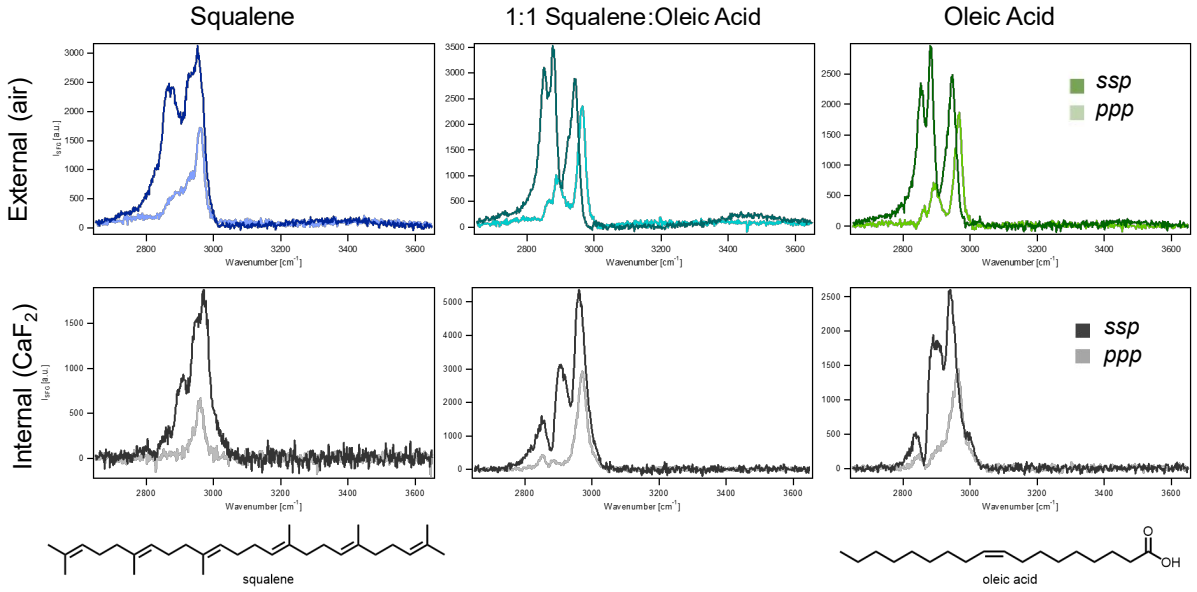

Figure 4.2: *ssp*- (dark) and *ppp*-polarized (light) external (top) and internal (bottom) reflection SFG spectra of squalene (left) and oleic acid (right) and a 1:1 mixture of both on CaF_2 (center)

Also present in the external spectra is a broad peak occurring at roughly 3400 cm^{-1}, corresponding to hydrogen-bonded -O-H groups resulting from adsorbed water. The lack of a similar peak in the internal reflection spectra may indicate that at typical RH levels i.e. 10-40% and STP, water

does not fully penetrate the monolayer of oleic acid/squalene deposited onto CaF_2. The lack of a similar peak in the internal reflection spectra may indicate that at typical RH levels i.e. 10-40% and STP, water does not fully penetrate the monolayer of oleic acid/squalene deposited onto CaF_2. It is possible that at high RH and extended exposure time water signal could be observed in internal reflection geometry using the flow setup from Chapter 3.

After gaining some insight into the surface partitioning behavior of oleic acid and squalene, we narrowed our focus on investing SFG signal at different mixing ratios of the two compounds. While the SFG spectrum of both oleic acid and squalene on silica (Figure 4.2) differ from those on CaF_2, oleic acid still displays 3 characteristic peaks while squalene displays two. Three peaks indicative of oleic acid signal are clearly visible in the mixed samples on the left side of Figure 4.2. The samples with higher squalene fractions on the right display two dominant peaks but are still affected by the oleic acid fraction.

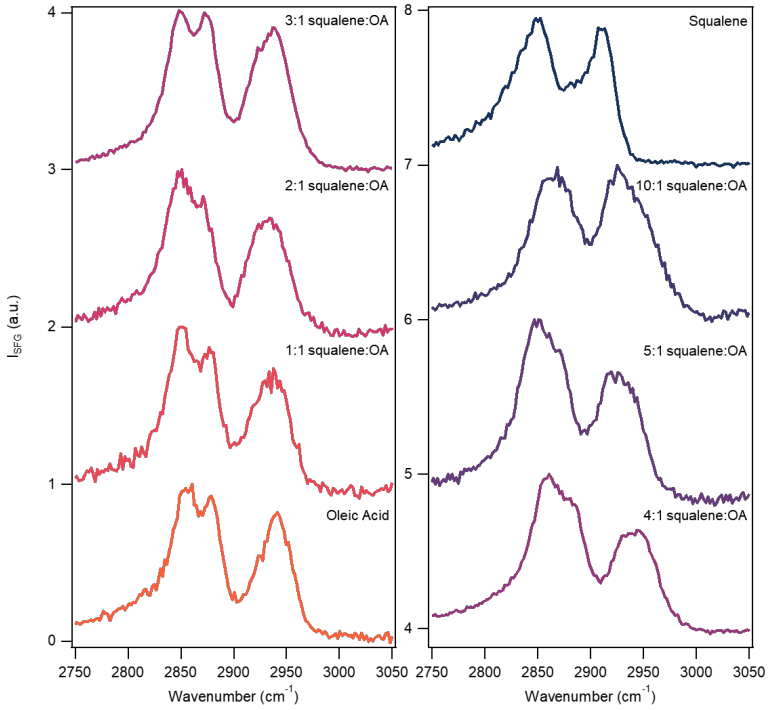

Figure 4.3: *sp*-polarized SFG spectra of squalene and oleic acid mixtures on silica.

The SFG spectrum of the pure squalene sample has two clear peaks at approximately 2855 cm^{-1} and 2915 cm^{-1}. However, it is apparent in the 10:1 squalene:OA spectrum that the presence of oleic acid causes these peaks to be slightly red shifted from that of pure squalene. In the 5:1 and 4:1 sample spectra, the peak at 2855 cm^{-1} has a shoulder reminiscent of the third characteristic oleic acid peak. By analyzing these mixtures of squalene and oleic acid using SFG spectroscopy, we hypothesized that there would be a ratio of the two where squalene would be present in high enough concentrations to dominate the air interface signal.

4.3.2 Scattering Experiments Show No Mixing Hole

Overall, the intensity of the scattered light remained constant relative to the mixing ratio. We would expect to see the intensity of the scattered light to increase dramatically with new phase formation. Taken together with the SFG experiments, the data indicate a pure surface (as opposed to bulk phase separation) phenomenon supporting the notion that squalene acts as a surfactant when mixed with oleic acid. These bulk measurements do not indicate a preference of oleic acid to phase separate.

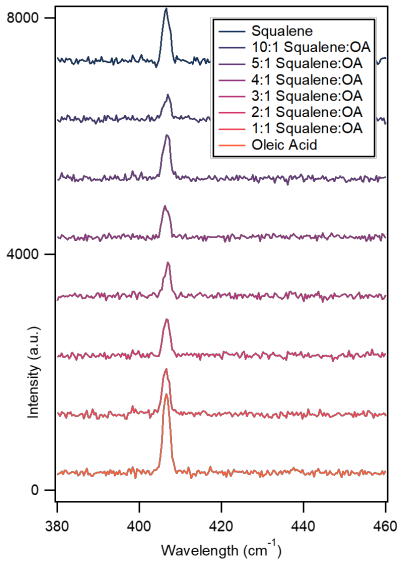

Figure 4.4: Scattering analysis of squalene and oleic acid binary mixtures.

References

1. Klepeis, N. E.; Nelson, W. C.; Ott, W. R.; Robinson, J. P.; Tsang, A. M.; Switzer, P.; Behar, J. V.; Hern, S. C.; Engelmann, W. H., The National Human Activity Pattern Survey (NHAPS): a resource for assessing exposure to environmental pollutants. *J Expo Anal Env Epid* **2001,** *11* (3), 231-252.

2. Wallace, L. A.; Pellizzari, E. D.; Hartwell, T. D.; Sparacino, C.; Whitmore, R.; Sheldon, L.; Zelon, H.; Perritt, R., The Team Study - Personal Exposures to Toxic-Substances in Air, Drinking-Water, and Breath of 400 Residents of New-Jersey, North-Carolina, and North-Dakota. *Environ Res* **1987,** *43* (2), 290-307.

3. Weschler, C. J., Ozone's impact on public health: contributions from indoor exposures to ozone and products of ozone-initiated chemistry. *Environ Health Perspect* **2006,** *114* (10), 1489-96.

4. Hoskins, J. A., Health Effects due to Indoor Air Pollution. *Indoor and Built Environment* **2016,** *12* (6), 427-433.

5. Manuja, A.; Ritchie, J.; Buch, K.; Wu, Y.; Eichler, C. M. A.; Little, J. C.; Marr, L. C., Total surface area in indoor environments. *Environ Sci Process Impacts* **2019,** *21* (8), 1384-1392.

6. Bouhamra, W. S.; Elkilani, A. S., Investigation and modeling of surface sorption/desorption behavior of volatile organic compounds for indoor air quality analysis. *Environmental Technology* **1999,** *20* (5), 531-545.

7. Bouhamra, W.; Elkilani, A., Development of a model for the estimation of indoor volatile organic compounds concentration based on experimental sorption parameters. *Environmental Science & Technology* **1999,** *33* (12), 2100-2105.

8. Elkilani, A.; Bouhamra, W.; Crittenden, B. D., An indoor air quality model that includes the sorption of VOCs on fabrics. *Process Safety and Environmental Protection* **2001,** *79* (B4), 233-243.

9. Molhave, L., The Sick Buildings and Other Buildings with Indoor Climate Problems. *Environ. Int.* **1989,** *15* (1-6), 65-74.

10. Weschler, C. J.; Hodgson, A. T.; Wooley, J. D., Indoor Chemistry - Ozone, Volatile Organic-Compounds, and Carpets. *Environmental Science & Technology* **1992,** *26* (12), 2371-2377.

11. Ekberg, L. E., Relationships between indoor and outdoor contaminants in mechanically ventilated buildings. *Indoor Air-International Journal of Indoor Air Quality and Climate* **1996,** *6* (1), 41-47.

12. Weschler, C. J.; Shields, H. C., Potential reactions among indoor pollutants. *Atmospheric Environment* **1997,** *31* (21), 3487-3495.

13. Bruce, N.; Perez-Padilla, R.; Albalak, R., Indoor air pollution in developing countries: a major environmental and public health challenge. *B World Health Organ* **2000,** *78* (9), 1078-1092.

14. Spengler, J. D.; Chen, Q. Y., Indoor air quality factors in designing a healthy building. *Annu. Rev. Energ. Environ.* **2000,** *25*, 567-600.

15. Fisk, W. J., Health and productivity gains from better indoor environments and their relationship with building energy efficiency. *Annu. Rev. Energy Environ.* **2000,** *25*, 537-566.

16. Shaughnessy, R. J.; McDaniels, T. J.; Weschler, C. J., Indoor chemistry: Ozone and volatile organic compounds found in tobacco smoke. *Environmental Science & Technology* **2001,** *35* (13), 2758-2764.

17. Nazaroff, W. W.; Weschler, C. J.; Corsi, R. L., Indoor air chemistry and physics. *Atmospheric Environment* **2003,** *37* (39-40), 5451-5453.

18. Patino, E. D. L.; Siegel, J. A., Indoor environmental quality in social housing: A literature review. *Building and Environment* **2018,** *131*, 231-241.

19. Wolkoff, P., Indoor air humidity, air quality, and health – An overview. *International Journal of Hygiene and Environmental Health* **2018,** *221* (3), 376-390.

20. Rubasinghege, G.; Grassian, V., Role(s) of Adsorbed Water in the Surface Chemistry of Environmental Interfaces. *Chem. Comm.* **2013,** *49*, 3071-94.

21. Morrison, G., Recent Advances in Indoor Chemistry. *Current Sustainable/Renewable Energy Reports* **2015,** *2* (2), 33-40.

22. Zhou, S. M.; Forbes, M. W.; Abbatt, J. P. D., Application of Direct Analysis in Real Time-Mass Spectrometry (DART-MS) to the Study of Gas-Surface Heterogeneous Reactions: Focus on Ozone and PAHs. *Analytical Chemistry* **2015,** *87* (9), 4733-4740.

23. Zhou, S. M.; Forbes, M. W.; Abbatt, J. P. D., Kinetics and Products from Heterogeneous Oxidation of Squalene with Ozone. *Environmental Science & Technology* **2016,** *50* (21), 11688-11697.

24. Zhou, S. M.; Forbes, M. W.; Katrib, Y.; Abbatt, J. P. D., Rapid Oxidation of Skin Oil by Ozone. *Environmental Science & Technology Letters* **2016,** *3* (4), 170-174.

25. Zhou, S. M.; Yeung, L. W. Y.; Forbes, M. W.; Mabury, S.; Abbatt, J. P. D., Epoxide formation from heterogeneous oxidation of benzo a pyrene with gas-phase ozone and indoor air. *Environmental Science-Processes & Impacts* **2017,** *19* (10), 1292-1299.

26. Or, V. W.; Alves, M. R.; Wade, M.; Schwab, S.; Corsi, R. L.; Grassian, V. H., Crystal Clear? Microspectroscopic Imaging and Physicochemical Characterization of Indoor Depositions on Window Glass. *Environ Sci Tech Let* **2018,** *5* (8), 514-519.

27. Collins, D. B.; Hems, R. F.; Zhou, S. M.; Wang, C.; Grignon, E.; Alavy, M.; Siegel, J. A.; Abbatt, J. P. D., Evidence for Gas-Surface Equilibrium Control of Indoor Nitrous Acid. *Environmental Science & Technology* **2018,** *52* (21), 12419-12427.

28. Alwarda, R.; Zhou, S.; Abbatt, J. P. D., Heterogeneous oxidation of indoor surfaces by gas-phase hydroxyl radicals. *Indoor Air* **2018,** *28* (5), 655-664.

29. Heine, N.; Arata, C.; Goldstein, A. H.; Houle, F. A.; Wilson, K. R., Multiphase Mechanism for the Production of Sulfuric Acid from SO2 by Criegee Intermediates Formed During the Heterogeneous Reaction of Ozone with Squalene. *Journal of Physical Chemistry Letters* **2018,** *9* (12), 3504-3510.

30. Fang, Y.; Lakey, P.; Riahi, S.; McDonald, A.; Shrestha, M.; Tobias, D. J.; Grassian, V. H., A Molecular Picture of Surface Interactions of Organic Compounds on Prevalent Indoor Surfaces: Limonene Adsorption on SiO2. *Chem. Sci.* **2019,** *10*, 2906-14.

31. Fang, Y.; Riahi, S.; McDonald, A. T.; Shrestha, M.; Tobias, D. J.; Grassian, V. H., What Is the Driving Force behind the Adsorption of Hydrophobic Molecules on Hydrophilic Surfaces? *The Journal of Physical Chemistry Letters* **2019,** *10* (3), 468-473.

32. Duncan, S. M.; Sexton, K. G.; Turpin, B. J., Oxygenated VOCs, aqueous chemistry, and potential impacts on residential indoor air composition. *Indoor Air* **2018,** *28* (1), 198-212.

33. Duncan, S. M.; Tomaz, S.; Morrison, G.; Webb, M.; Atkin, J.; Surratt, J. D.; Turpin, B. J., Dynamics of Residential Water-Soluble Organic Gases: Insights into Sources and Sinks. *Environmental Science & Technology* **2019,** *53* (4), 1812-1821.

34. Farmer, D. K.; Vance, M. E.; Abbatt, J. P. D.; Abeleira, A.; Alves, M. R.; Arata, C.; Boedicker, E.; Bourne, S.; Cardoso-Saldaña, F.; Corsi, R.; DeCarlo, P. F.; Goldstein, A. H.; Grassian, V. H.; Hildebrandt Ruiz, L.; Jimenez, J. L.; Kahan, T. F.; Katz, E. F.; Mattila, J. M.; Nazaroff, W. W.; Novoselac, A.; O'Brien, R. E.; Or, V. W.; Patel, S.; Sankhyan, S.; Stevens, P. S.; Tian, Y.; Wade, M.; Wang, C.; Zhou, S.; Zhou, Y., Overview of HOMEChem: House Observations of Microbial and Environmental Chemistry. *Environmental Science: Processes & Impacts* **2019,** *21* (8), 1280-1300.

35. Zhou, Z.; Zhou, S.; Abbatt, J. P. D., Kinetics and Condensed-Phase Products in Multiphase Ozonolysis of an Unsaturated Triglyceride. *Environmental Science & Technology* **2019,** *53* (21), 12467-12475.

36. Schwartz-Narbonne, H.; Wang, C.; Zhou, S.; Abbatt, J. P. D.; Faust, J., Heterogeneous Chlorination of Squalene and Oleic Acid. *Environmental Science & Technology* **2019,** *53* (3), 1217-1224.

37. Weschler, C. J., Roles of the human occupant in indoor chemistry. *Indoor Air* **2016,** *26* (1), 6-24.

38. Wisthaler, A.; Weschler, C. J., Reactions of ozone with human skin lipids: sources of carbonyls, dicarbonyls, and hydroxycarbonyls in indoor air. *Proc Natl Acad Sci U S A* **2010,** *107* (15), 6568-75.

39. Dormont, L.; Bessière, J.-M.; Cohuet, A., Human Skin Volatiles: A Review. *Journal of Chemical Ecology* **2013,** *39* (5), 569-578.

40. Fenske, J. D.; Paulson, S. E., Human Breath Emissions of VOCs. *Journal of the Air & Waste Management Association* **1999,** *49* (5), 594-598.

41. Kruza, M.; Carslaw, N., How do breath and skin emissions impact indoor air chemistry? *Indoor Air* **2019,** *29* (3), 369-379.

42. Coffaro, B.; Weisel, C. P., Reactions and Products of Squalene and Ozone: A Review. *Environ Sci Technol* **2022,** *56* (12), 7396-7411.

43. Zhang, M.; Xiong, J.; Liu, Y.; Misztal, P. K.; Goldstein, A. H., Physical–Chemical Coupling Model for Characterizing the Reaction of Ozone with Squalene in Realistic Indoor Environments. *Env. Sci. Technol.* **2021,** *55*, 1690-8.

44. Petrick, L.; Dubowski, Y., Heterogeneous oxidation of squalene film by ozone under various indoor conditions. *Indoor Air* **2009,** *19* (5), 381-391.

45. Fu, D.; Leng, C. B.; Kelley, J.; Zeng, G.; Zhang, Y. H.; Liu, Y., ATR-IR Study of Ozone Initiated Heterogeneous Oxidation of Squalene in an Indoor Environment. *Environmental Science & Technology* **2013,** *47* (18), 10611-10618.

46. Arata, C.; Heine, N.; Wang, N.; Misztal, P. K.; Wargocki, P.; Beko, G.; Williams, J.; Nazaroff, W. W.; Wilson, K. R.; Goldstein, A. H., Heterogeneous Ozonolysis of Squalene: Gas-Phase Products Depend on Water Vapor Concentration. *Environ Sci Technol* **2019,** *53* (24), 14441-14448.

47. Shimizu, N.; Ito, J.; Kato, S.; Otoki, Y.; Goto, M.; Eitsuka, T.; Miyazawa, T.; Nakagawa, K., Oxidation of squalene by singlet oxygen and free radicals results in different compositions of squalene monohydroperoxide isomers. *Sci Rep-Uk* **2018,** *8*.

48. Zhou, S.; Forbes, M. W.; Abbatt, J. P. D., Kinetics and Products from Heterogeneous Oxidation of Squalene with Ozone. *Env. Sci. Technol.* **2016,** *50*, 11688-97.

49. Anderson, S. E.; Franko, J.; Jackson, L. G.; Wells, J. R.; Ham, J. E.; Meade, B. J., Irritancy and allergic responses induced by exposure to the indoor air chemical 4-oxopentanal. *Toxicol Sci* **2012,** *127* (2), 371-81.

50. Naziri, E.; Consonni, R.; Tsimidou, M. Z., Squalene oxidation products: Monitoring the formation, characterisation and pro-oxidant activity. *Eur J Lipid Sci Tech* **2014,** *116* (10), 1400-1411.

51. Zhang, M.; Gao, Y.; Xiong, J., Characterization of the off-body squalene ozonolysis on indoor surfaces. *Chemosphere* **2022,** *291* (Pt 1), 132772.

52. Zhou, S.; Forbes, M. W.; Katrib, Y.; Abbatt, J. P. D., Rapid Oxidation of Skin Oil by Ozone. *Env. Sci. Technol. Lett.* **2016,** *3*, 170-4.

53. Boyd, R. W., *Nonlinear Optics, 3rd Edition*. Elsevier Academic Press Inc: San Diego, 2008; p 1-613.

54. Shen, Y. R., *The Principles of Nonlinear Optics*. John Wiley & Sons, Inc.: Hoboken, NJ, 2003.

55. Morita, A., *Theory of Sum Frequency Generation Spectroscopy*. Springer: 2018; Vol. 97.

56. Mukamel, S., *Principles of Nonlinear Optical Spectroscopy*. Oxford University Press: Oxford, 1995.

57. Zhuang, X.; Miranda, P. B.; Kim, D.; Shen, Y. R., Mapping molecular orientation and conformation at interfaces by surface nonlinear optics. *Phys Rev B* **1999,** *59* (19), 12632-12640.

58. Wang, H.-F.; Gan, W.; Lu, R.; Rao, Y.; Wu, B.-H., Quantitative spectral and orientational analysis in surface sum frequency generation vibrational spectroscopy (SFG-VS). *International Reviews in Physical Chemistry* **2005,** *24* (2), 191-256.

59. Stokes, G. Y.; Buchbinder, A. M.; Gibbs-Davis, J. M.; Scheidt, K. A.; Geiger, F. M., Chemically diverse environmental interfaces and their reactions with ozone studied by sum frequency generation. *Vibrational Spectroscopy* **2009,** *50* (1), 86-98.

60. Buchbinder, A. M.; Gibbs-Davis, J. M.; Stokes, G. Y.; Peterson, M. D.; Weitz, E.; Geiger, F. M., Method for Evaluating Vibrational Mode Assignments in Surface-Bound Cyclic Hydrocarbons Using Sum-Frequency Generation. *The Journal of Physical Chemistry C* **2011,** *115* (37), 18284-18294.

61. Lu, R.; Gan, W.; Wu, B.-h.; Zhang, Z.; Guo, Y.; Wang, H.-f., C−H Stretching Vibrations of Methyl, Methylene and Methine Groups at the Vapor/Alcohol (n = 1−8) Interfaces. *The Journal of Physical Chemistry B* **2005,** *109* (29), 14118-14129.

62. Stokes, G. Y.; Buchbinder, A. M.; Gibbs-Davis, J. M.; Scheidt, K. A.; Geiger, F. M., Heterogenous Ozone Oxidation Reactions of 1-Pentene, Cyclopentene, Cyclohexene, and Menthenol Derivative Studied by Sum Frequency Generation. *J. Phys. Chem. A* **2008,** *112*, 11688-11698.

63. Voges, A. B.; Stokes, G. Y.; Gibbs-Davis, J. M.; Lettan, R. B.; Bertin, P. A.; Pike, R. C.; Nguyen, S. T.; Sheidt, K. A.; Geiger, F. M., Insights into Heterogeneous Atmospheric Oxidation Chemistry: Development of a Tailor-Made Synthetic Model for Studying Tropospheric Surface Chemistry. *J. Phys. Chem. C* **2007,** *111*, 1567-1578.

64. Voges, A. B.; Al-Abadleh, H. A.; Musorrariti, M. J.; Bertin, P. A.; Nguyen, S. T.; Geiger, F. M., Carboxylic acid- and ester-functionalized siloxane scaffolds on glass studied by broadband sum frequency generation. *Journal of Physical Chemistry B* **2004,** *108* (48), 18675-18682.

65. von Domaros, M.; Liu, Y.; Butman, J. L.; Perlt, E.; Geiger, F. M.; Tobias, D. J., Molecular Orientation at the Squalene/Air Interface from Sum Frequency Generation Spectroscopy and Atomistic Modeling. *The Journal of Physical Chemistry B* **2021,** *125*, 3932-41.

66. Ma, E.; Ohno, P. E.; Kim, K.; Liu, Y.; Lozier, E. H.; Miller III, T. F.; Wang, H.-f.; Geiger, F. M., A New Imaginary Term in the 2nd Order Nonlinear Susceptibility from Charged Interfaces. *J. Phys. Chem. Lett.* **2021,** *12* (24), 5649-59.

67. Stokes, G. Y.; Chen, E. H.; Buchbinder, A. M.; Paxton, W. F.; Keeley, A.; Geiger, F. M., Atmospheric Heterogeneous Stereochemistry. *Journal of the American Chemical Society* **2009,** *131* (38), 13733-13737.

68. Stokes, G. Y.; Chen, E. H.; Walter, S. R.; Geiger, F. M., Two Reactivity Modes in the Heterogeneous Cyclohexene Ozonolysis under Tropospherically Relevant Ozone-Rich and Ozone-Limited Conditions. *The Journal of Physical Chemistry A* **2009,** *113* (31), 8985-8993.

69. Stokes, G. Y.; Buchbinder, A. M.; Gibbs-Davis, J. M.; Scheidt, K. A.; Geiger, F. M., Heterogeneous Ozone Oxidation Reactions of 1-Pentene, Cyclopentene, Cyclohexene, and a Menthenol Derivative Studied by Sum Frequency Generation. *The Journal of Physical Chemistry A* **2008,** *112* (46), 11688-11698.

70. Lawrence, C. P.; Skinner, J. L., Ultrafast infrared spectroscopy probes hydrogen-bonding dynamics in liquid water. *Chemical Physics Letters* **2003,** *369* (3), 472-477.

71. Sefler, G. A.; Du, Q.; Miranda, P. B.; Shen, Y. R., Surface Crystallization of Liquid N-Alkanes and Alcohol Monolayers Studied by Surface Vibrational Spectroscopy. *Chemical Physics Letters* **1995,** *235* (3-4), 347-354.

72. Kliewer, C. J.; Bieri, M.; Somorjai, G. A., Hydrogenation of the α,β-Unsaturated Aldehydes Acrolein, Crotonaldehyde, and Prenal over Pt Single Crystals: A Kinetic and Sum-Frequency Generation Vibrational Spectroscopy Study. *Journal of the American Chemical Society* **2009,** *131* (29), 9958-9966.

73. Michalak, W. D.; Krier, J. M.; Komvopoulos, K.; Somorjai, G. A., Structure Sensitivity in Pt Nanoparticle Catalysts for Hydrogenation of 1,3-Butadiene: In Situ Study of Reaction Intermediates Using SFG Vibrational Spectroscopy. *The Journal of Physical Chemistry C* **2013,** *117* (4), 1809-1817.

74. Kennedy, G.; Melaet, G.; Han, H.-L.; Ralston, W. T.; Somorjai, G. A., In Situ Spectroscopic Investigation into the Active Sites for Crotonaldehyde Hydrogenation at the Pt Nanoparticle–Co3O4 Interface. *ACS Catalysis* **2016,** *6* (10), 7140-7147.

75. Walter, S. R.; Youn, J.; Emery, J. D.; Kewalramani, S.; Hennek, J. W.; Bedzyk, M. J.; Facchetti, A.; Marks, T. J.; Geiger, F. M., In-Situ Probe of Gate Dielectric-Semiconductor Interfacial Order in Organic Transistors: Origin and Control of Large Performance Sensitivities. *Journal of the American Chemical Society* **2012,** *134* (28), 11726-11733.

76. Chun, H. J.; Weiss, T. L.; Devarenne, T. P.; Laane, J., Vibrational spectra and DFT calculations of squalene. *Journal of Molecular Structure* **2013,** *1032*, 203-206.

77. Hall, D. W.; Marshall, S. N.; Gordon, K. C.; Killeen, D. P., Rapid Quantitative Determination of Squalene in Shark Liver Oils by Raman and IR Spectroscopy. *Lipids* **2016,** *51* (1), 139-147.

78. Upshur, M. A.; Chase, H. M.; Strick, B. F.; Ebben, C. J.; Fu, L.; Wang, H.; Thomson, R. J.; Geiger, F. M., Vibrational Mode Assignment of α-Pinene by Isotope Editing: One Down, Seventy-One To Go. *The Journal of Physical Chemistry A* **2016,** *120* (17), 2684-2690.

79. Buchy, E.; Vukosavljevic, B.; Windbergs, M.; Sobot, D.; Dejean, C.; Mura, S.; Couvreur, P.; Desmaële, D., Synthesis of a deuterated probe for the confocal Raman microscopy imaging of squalenoyl nanomedicines. *Beilstein Journal of Organic Chemistry* **2016,** *12*, 1127-1135.

80. Chase, H. M.; Psciuk, B. T.; Strick, B. L.; Thomson, R. J.; Batista, V. S.; Geiger, F. M., Beyond Local Group Modes in Vibrational Sum Frequency Generation. *The Journal of Physical Chemistry A* **2015,** *119* (14), 3407-3414.

81. Baryiames, C. P.; Baiz, C. R., Slow Oil, Slow Water: Long-Range Dynamic Coupling across a Liquid–Liquid Interface. *Journal of the American Chemical Society* **2020,** *142* (18), 8063-8067.

82. Shrestha, M.; Zhang, Y.; Upshur, M. A.; Liu, P.; Blair, S. L.; Wang, H.-f.; Nizkorodov, S. A.; Thomson, R. J.; Martin, S. T.; Geiger, F. M., On Surface Order and Disorder of α-Pinene-Derived Secondary Organic Material. *The Journal of Physical Chemistry A* **2015,** *119* (19), 4609-4617.

83. Kidd, C.; Perraud, V.; Wingen, L. M.; Finlayson-Pitts, B. J., Integrating phase and composition of secondary organic aerosol from the ozonolysis of α-pinene. *Proceedings of the National Academy of Sciences* **2014,** *111* (21), 7552.

84. Liu, Y.; Bé, A. G.; Or, V. W.; Alves, M. R.; Grassian, V. H.; Geiger, F. M., Challenges and Opportunities in Molecular-Level Indoor Surface Chemistry and Physics. *Cell Reports Physical Science* **2020,** *1* (11).

85. Farmer, D. K., Analytical Challenges and Opportunities For Indoor Air Chemistry Field Studies. *Anal Chem* **2019,** *91* (6), 3761-3767.

86. Farmer, D. K.; Vance, M. E.; Abbatt, J. P. D.; Abeleira, A.; Alves, M. R.; Arata, C.; Boedicker, E.; Bourne, S.; Cardoso-Saldana, F.; Corsi, R.; DeCarlo, P. F.; Goldstein, A. H.; Grassian, V. H.; Hildebrandt Ruiz, L.; Jimenez, J. L.; Kahan, T. F.; Katz, E. F.; Mattila, J. M.; Nazaroff, W. W.; Novoselac, A.; O'Brien, R. E.; Or, V. W.; Patel, S.; Sankhyan, S.; Stevens, P. S.; Tian, Y.; Wade, M.; Wang, C.; Zhou, S.; Zhou, Y., Overview of HOMEChem: House Observations of Microbial and Environmental Chemistry. *Environ Sci Process Impacts* **2019,** *21* (8), 1280-1300.

87. Fiegland, L. R.; Saint Fleur, M. M.; Morris, J. R., Reactions of C=C-terminated self-assembled monolayers with gas-phase ozone. *Langmuir* **2005,** *21* (7), 2660-2661.

88. Lu, J. W.; Fiegland, L. R.; Davis, E. D.; Alexander, W. A.; Wagner, A.; Gandour, R. D.; Morris, J. R., Initial Reaction Probability and Dynamics of Ozone Collisions with a Vinyl-Terminated Self-Assembled Monolayer. *J Phys Chem C* **2011,** *115* (51), 25343-25350.

89. Athanasiadis, A.; Fitzgerald, C.; Davidson, N. M.; Giorio, C.; Botchway, S. W.; Ward, A. D.; Kalberer, M.; Pope, F. D.; Kuimova, M. K., Dynamic viscosity mapping of the oxidation of squalene aerosol particles. *Physical Chemistry Chemical Physics* **2016,** *18* (44), 30385-30393.

90. Fooshee, D. R.; Aiona, P. K.; Laskin, A.; Laskin, J.; Nizkorodov, S. A.; Baldi, P. F., Atmospheric Oxidation of Squalene: Molecular Study Using COBRA Modeling and High-Resolution Mass Spectrometry. *Environmental Science & Technology* **2015,** *49* (22), 13304-13313.

91. Jacobs, M. I.; Xu, B.; Kostko, O.; Heine, N.; Ahmed, M.; Wilson, K. R., Probing the Heterogeneous Ozonolysis of Squalene Nanoparticles by Photoemission. *J Phys Chem A* **2016,** *120* (43), 8645-8656.

92. Lakey, P. S. J.; Morrison, G. C.; Won, Y.; Parry, K. M.; von Domaros, M.; Tobias, D. J.; Rim, D.; Shiraiwa, M., The impact of clothing on ozone and squalene ozonolysis products in indoor environments. *Communications Chemistry* **2019,** *2* (1).

93. Liu, L.; Chase, H. M.; Geiger, F. M., Partially (resp. fully) reversible adsorption of monoterpenes (resp. alkanes and cycloalkanes) to fused silica. *J. Chem. Phys. Feature Article* **2019,** *150*, 074701.

94. Chase, H. M.; Ho, J.; Upshur, M. A.; Thomson, R. J.; Batista, V. S.; Geiger, F. M., Unanticipated Stickiness of α-Pinene. *J. Phys. Chem. A* **2017,** *121* (17), 3239–3246.

95. Kruza, M.; Lewis, A. C.; Morrison, G. C.; Carslaw, N., Impact of surface ozone interactions on indoor air chemistry: A modeling study. *Indoor Air* **2017,** *27*, 1001-11.

96. Xiong, J.; He, Z.; Tang, X.; Misztal, P. K.; Goldstein, A. H., Modeling the Time-Dependent Concentrations of Primary and Secondary Reaction Products of Ozone with Squalene in a University Classroom. *Env. Sci. & Technol.* **2019,** *53*, 8262-70.

97. Stokes, G. Y.; Chen, E. H.; Walter, S. R.; Geiger, F. M., Two Reactivity Modes in the Heterogeneous Cyclohexene Ozonolysis under Tropospherically Relevant Ozone-Rich and Ozone-Limited Conditions. *J. Phys. Chem. A* **2009,** *113* (31), 8985-8993.

98. Butman, J. L.; Thomson, R. J.; Geiger, F. M., Unanticipated Hydrophobicity Increases of Squalene and Human Skin Oil Films Upon Ozone Exposure. *J Phys Chem B* **2022,** *126* (45), 9417-9423.

99. Majumder, M.; Rendall, C. S.; Eukel, J. A.; Wang, J. Y.; Behabtu, N.; Pint, C. L.; Liu, T. Y.; Orbaek, A. W.; Mirri, F.; Nam, J.; Barron, A. R.; Hauge, R. H.; Schmidt, H. K.; Pasquali, M., Overcoming the "coffee-stain" effect by compositional Marangoni-flow-assisted drop-drying. *J Phys Chem B* **2012,** *116* (22), 6536-42.

100. Murisic, N.; Kondic, L., On evaporation of sessile drops with moving contact lines. *Journal of Fluid Mechanics* **2011,** *679*, 219-246.

101. Stokes, G. Y.; Chen, E. H.; Walter, S. R.; Geiger, F. M., Two Reactivity Modes in the Heterogeneous Cyclohexene Ozonolysis under Tropospherically Relevant Ozone-Rich and Ozone-Limited Conditions. *Journal of Physical Chemistry A* **2009,** *113* (31), 8985-8993.

102. Stokes, G. Y.; Buchbinder, A. M.; Gibbs-Davis, J. M.; Scheidt, K. A.; Geiger, F. M., Heterogeneous Ozone Oxidation Reactions of 1-Pentene, Cyclopentene, Cyclohexene, and a Menthenol Derivative Studied by Sum Frequency Generation. *Journal of Physical Chemistry A* **2008,** *112* (46), 11688-11698.

103. McIntire, T. M.; Lea, S. A.; Gaspar, D. J.; Jaitly, N.; Dubowski, Y.; Li, Q.; Finlayson-Pitts, B. J., Unusual aggregates from the oxidation of alkene self-assembled monolayers: a previously unrecognized mechanism for SAM ozonolysis? *PCCP* **2006,** *7*, 3605-3609.

104. please visit https://www.profilmonline.com. **2022**.

105. Xu, S.; Mahrt, F.; Gregson, F. K. A.; Bertram, A. K., Possible Effects of Ozone Chemistry on the Phase Behavior of Skin Oil and Cooking Oil Films and Particles Indoors. *ACS Earth and Space Chemistry* **2022**.

106. Sangster, J., Octanol-Water Partition Coefficients of Simple Organic Compounds. *J. Phys. Chem. Ref. Data* **1989,** *18*, 1111-1227.

107. DuPre, D. B.; Yappert, M. C., Cooperative Hydrogen- and πH-Bonded Interactions Involving Water and the Ethylenic Double Bond. *J. Phys. Chem. A* **2002,** *106*, 567-74.

108. Angdahl, A.; Nelander, B., Water-olefin complexes. A matrix isolation study. *J. Phys. Chem.* **1986,** *90*, 4982-7.

109. Nicolaides, N., Skin Lipids - Their Biochemical Uniqueness. *Science* **1974,** *186* (4158), 19-26.

110. von Domaros, M.; Liu, Y.; Butman, J. L.; Perlt, E.; Geiger, F. M.; Tobias, D. J., Molecular Orientation at the Squalene/Air Interface from Sum Frequency Generation Spectroscopy and Atomistic Modeling. *The Journal of Physical Chemistry B* **2021**.

111. Morrison, G. C.; Eftekhari, A.; Majluf, F.; Krechmer, J. E., Yields and Variability of Ozone Reaction Products from Human Skin. *Environ Sci Technol* **2021,** *55* (1), 179-187.

112. Zahardis, J.; Geddes, S.; Petrucci, G. A., The ozonolysis of primary aliphatic amines in fine particles. *Atmospheric Chemistry and Physics* **2008,** *8* (5), 1181-1194.

113. Pfrang, C.; Shiraiwa, M.; Poschl, U., Chemical ageing and transformation of diffusivity in semi-solid multi-component organic aerosol particles. *Atmospheric Chemistry and Physics* **2011,** *11* (14), 7343-7354.

114. Guenther, A. B.; Jiang, X.; Heald, C. L.; Sakulyanontvittaya, T.; Duhl, T.; Emmons, L. K.; Wang, X., The Model of Emissions of Gases and Aerosols from Nature version 2.1 (MEGAN2.1): an extended and updated framework for modeling biogenic emissions. *Geosci Model Dev* **2012,** *5* (6), 1471-1492.

115. Paulot, F.; Crounse, J. D.; Kjaergaard, H. G.; Kurten, A.; St Clair, J. M.; Seinfeld, J. H.; Wennberg, P. O., Unexpected Epoxide Formation in the Gas-Phase Photooxidation of Isoprene. *Science* **2009,** *325* (5941), 730-733.

116. Chase, H. M.; Rudshteyn, B.; Psciuk, B. T.; Upshur, M. A.; Strick, B. F.; Thomson, R. J.; Batista, V. S.; Geiger, F. M., Assessment of DFT for Computing Sum Frequency Generation Spectra of an Epoxydiol and a Deuterated Isotopologue at Fused Silica/Vapor Interfaces. *Journal of Physical Chemistry B* **2016,** *120* (8), 1919-1927.

117. Ebben, C. J.; Martinez, I. S.; Shrestha, M.; Buchbinder, A. M.; Corrigan, A. L.; Guenther, A.; Karl, T.; Petaja, T.; Song, W. W.; Zorn, S. R.; Artaxo, P.; Kulmala, M.; Martin, S. T.; Russell, L. M.; Williams, J.; Geiger, F. M., Contrasting organic aerosol particles from boreal and tropical forests during HUMPPA-COPEC-2010 and AMAZE-08 using coherent vibrational spectroscopy. *Atmospheric Chemistry and Physics* **2011,** *11* (20), 10317-10329.

118. Varelas, J. G.; Vega, M. M.; Upshur, M. A.; Geiger, F. M.; Thomson, R. J., Synthesis Enabled Investigations into the Acidity and Stability of Atmospherically-Relevant Isoprene-Derived Organosulfates. *Acs Earth and Space Chemistry* **2022**.

Appendix A: SFG of Atmospheric Sulfates Derived from Isoprene

Mass-spectrometry has often been the workhorse characterization method relied upon for identifying secondary organic aerosol (SOA) material in field samples. However, conventional MS has the limitation of being unable to distinguish between different isomers of compounds with the same molecular weight. Several analytical methods have been identified to supplement MS. While different conformers can be distinguished using a mass spec technique known as X which differentiates based on cross-sectional area, it is necessary to cultivate a toolkit of different characterization methods. Certain compounds may be nonvolatile and thus ineligible candidates for MS analysis. SFG is presented in this appendix as a viable method for distinguishing different conformers based on surface orientation. This may be useful for benchmarking known compounds in field SOA studies.

For this study, we have chosen to analyze a suite of 8 sulfated SOA compounds with identical molecular weights. SOA have natural and anthropogenic origins and their impact on the environment and atmosphere is hypothesized to be significant, but not well understood. Around 500 Tg of the volatile organic compound (VOC) isoprene is estimated to be emitted annually by vegetation, constituting ~50% of biogenic VOC emissions overall.[114] Isoprene can undergo photooxidation with hydroxyl radicals in the environment to form secondary organic material (SOM) known as isoprene-derived epoxydiols (IEPOX),[115] which then reacts with anthropogenic sulfur in the atmosphere to form organosulfates. The proposed reaction scheme of isoprene generating IEPOX, the tetraol **9** and **10**, and sulfated compounds **1-8** is shown in Figure 2. The characteristic mass of compounds **1-8** has been detected by a variety of laboratory and field studies, but the position of the sulfate ester is unknown.

Previous work has shown it is possible to do DFT calculations comparing the amplitudes of *ssp*- and *ppp*-polarized SFG spectra to discern bond orientation.[116] For compounds like those in figure

X with the same molecular weight, mass spec becomes less reliable. SFG has the advantage of being highly sensitive to samples even on the nanogram scale, which makes it an appealing technique for atmospheric field samples which can be very dilute.[117] In contrast to mass spectrometry, SFG is effective on nonvolatile specimens which is necessary for analysis of some particle phase analytes.

All observed compounds (Figure A.1) were synthesized according to procedures published previously.[118] Each compound was characterized using NMR prior to observation with SFG. Experiments utilized either the *sp* polarization combination (S-polarized SFG signal, S-polarized 800 nm visible, P-polarized IR), which observes the components of the vibrational transition dipole moments that are oriented perpendicular to the SiO_2 substrate, or the *ppp* polarization, which observes bonds oriented parallel to surface normal. The SFG spectra were calibrated to the 2850 cm^{-1} and 3060 cm^{-1} peaks of a polystyrene film placed in the IR beam (ICL crystal laboratories). SFG intensity was normalized to gold plus one to accurately represent SFG intensity and avoid exaggerating the noise below 2700 cm^{-1} or above 3100 cm^{-1}. The spectra reported are an average of 3 individual acquisitions each recorded for 2 minutes in order to achieve an acceptable signal-to-noise ratio. All experiments were performed at room temperature (21-23 ºC) and 30-35% relative humidity. All experiments were carried out in duplicate. All data was processed using IGOR software. Before each experiment, the fused silica optical windows (ISP Optics), the Teflon block, and the Viton o-rings were sonicated in methanol (Fisher Scientific, HPLC grade), rinsed with methanol and Millipore water alternately and dried with nitrogen gas. The windows, block, and o-rings were then plasma-cleaned for 10 minutes on high (18W) prior to acquisition (Harrick Plasma). All sulfate samples were prepared in 1mmol solution in 1mL of d4-methanol (Fisher Scientific) and spin coated dropwise onto fused silica at 3000 rpm over 10 minutes.

As shown in Figure A.1, the spectral signature of each compound can be qualitatively distinguished from each other. Compounds **1-8** share the same molecular weight and formula, while **9** and **10** represent the syn- and anti-configurations of the tetraol precursor. The polar sulfate ester group likely dictates the orientation of the molecule on the SiO_2 substrate, leading to differences in the SFG spectra of each compound that allow a certain degree of distinction between conformers. We do not fit our data because we have non-normal modes where symmetries aren't known. Orientational analysis is out. Instead, we can use SFG spectroscopy to find differences between constitutional isomers.

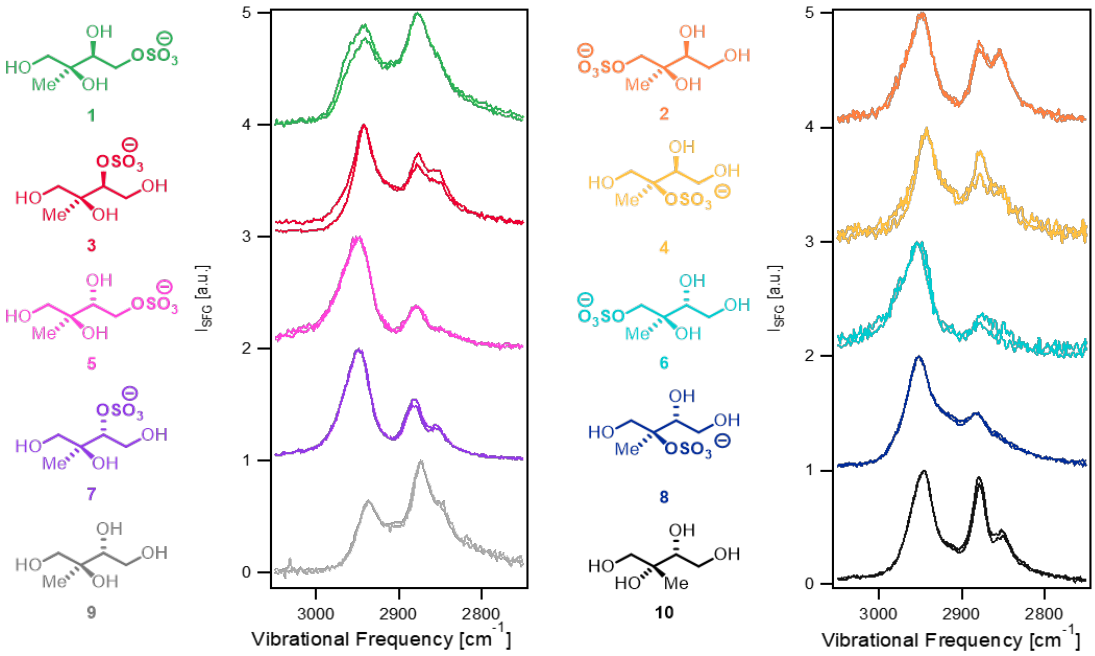

Figure A.1: Structures and *ssp*-polarized SFG spectra of the 10 isoprene derived compounds in this study.

The spectral signatures of 5, 6, and 8 bear strong similarities in peak intensity at 2950 and 2890 cm^{-1} with a potential third peak at 2850 cm^{-1} that has not resolved. Compound 1 can be distinguished from the group of sulfates due to the higher relative intensity of the peak at 2890 cm^{-1} compared to the 2950 cm^{-1} peak.

We chose to compare *ssp*- and *ppp*-polarized SFG spectra of 7 and 8, in Figure A.2 as we hypothesized that with the most hindered tertiary sulfate group their orientations would be most different from each other in differing polarization modes. We also believe that the tertiary substituted sulfate is the most likely isoprene-derived SOA structure based on the proposed reaction pathway of IEPOX in the presence of anthropogenic sulfur emissions.

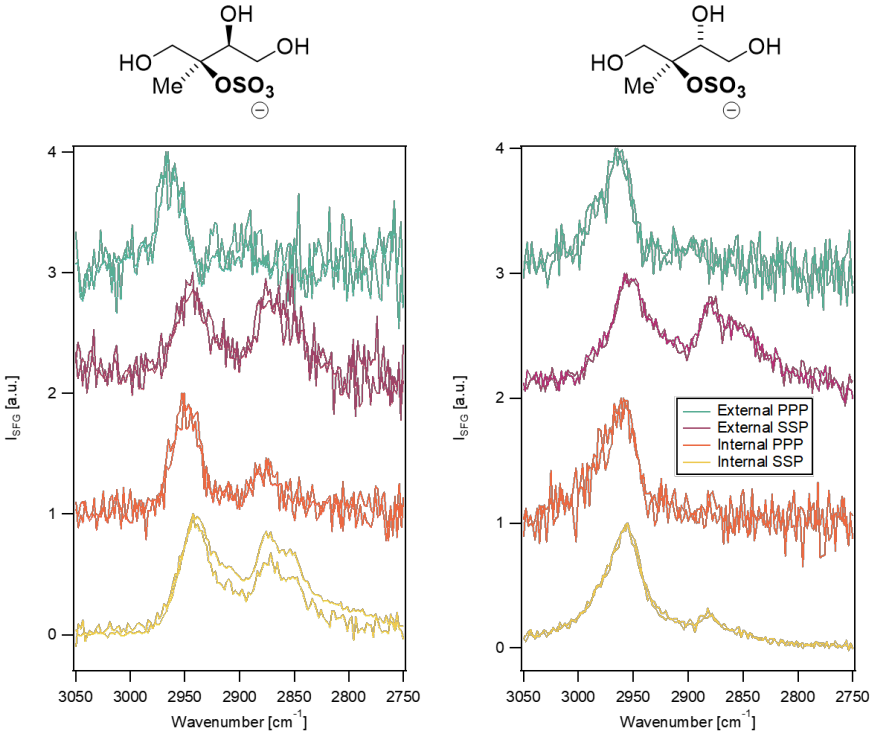

Figure A.2: Compounds 7 and 8 in external (air) and internal (silica) interfacial geometries, in *ppp* and *ssp* polarizations

While compounds 7 and 8 both show signal in the *ssp* region around 2890 cm^{-1} wavenumbers, the C-H bond giving rise to the peak at 2890 cm^{-1} in compound 8 is not visible in the *ppp* mode. Further orientational analysis using DFG, a methodology used previously in this lab[116] can lead to the identification of the vibrational mode responsible for this signal. Here we show that by changing the polarization mode of the SFG experiment, differences can be found between these sulfates due to how they are oriented on the surface of silica.

Jana Butman

703.887.1611 | janabutman@u.northwestern.edu | behance.net/janabutman

Education

Northwestern University | Doctor of Philosophy in Chemistry | Evanston, IL

Brown/RISD Dual Degree Program | Providence, RI
Brown University | Bachelor of Science in Chemistry
Rhode Island School of Design (RISD) | Bachelor of Fine Arts in Furniture Design

Research Experience

Northwestern University | Graduate Researcher | Evanston, IL 2018-present

- Researching the impact of human occupancy on indoor air pollution using surface-specific analysis including sum frequency generation (SFG) spectroscopy and optical profilometry
- Collaborated with the Tobias group at UC Irvine to publish on the surface reactivity of ozone with squalene
- Writing and editing grant proposals to fund further study of interfacial indoor atmospheric chemistry
- Managing lab safety including hazardous waste disposal, laboratory maintenance, and safety reviews/training

Library of Congress | Preservation Research and Testing Junior Fellow| Washington, DC | 2017

- Used XRF, IR, HPLC, and optical microscopy to analyze surface fouling on early recording media
- Successfully developed new cleaning formulations and methodology for digitizing wax cylinders
- Presented research to multiple audiences including tourists, scientists, and government officials

Brown University | Undergraduate Researcher | Providence, RI | 2016-2018

- Advised by Prof. Jerome Robinson. Synthesized novel organic ligands and lanthanide compounds
- Characterized products by NMR, MS, UV-VIS, and XRD

Skills

Laboratory Techniques
Contact Angle Goniometry, Energy Dispersive X-Ray Spectroscopy (EDS), Fourier-Transform Infrared Spectroscopy (FTIR), Liquid/Gas Chromatography-Mass Spectroscopy (LCMS/GCMS), Nonlinear Spectroscopy, Nuclear Magnetic Resonance Spectroscopy (NMR), Optical Microscopy,

Optical Profilometry, Organic and inorganic synthesis, Pendant Drop Interfacial Tension (IFT), Scanning Electron Microscopy (SEM), Sum Frequency Generation Spectroscopy (SFG), Transmission Electron Microscopy (TEM), Ultraviolet-Visual Spectroscopy (UV-VIS), X-Ray Fluorescence (XRF)

Software and Computer Aided Design
ChemDraw, IGOR, MestreNova, Microsoft Office (Word, Excel), Python, Adobe Creative Suite (Photoshop, Illustrator, InDesign), Autodesk (AutoCAD, Inventor, Revit), Dassault Systems (SolidWorks, MasterCam), GNU Image Manipulation Program (GIMP), Procreate

Studio Art and Museum
Bookbinding, Ceramics, Drawing, Metalworking, Painting, Printmaking, TIG Welding, Upholstering, Woodworking, Laser Cutting, Machining, Technical Drafting, Thermoforming, Art Handling, Art Installation, Crating, Framing, WAV Lift Operation, Vinyl Wrapping, 3D Printing

Arts Experience

Sloans & Kenyon Auctioneers and Appraisers | Art Department Intern | Chevy Chase, MD | 2016

- Researched and appraised consignors' paintings and works on paper
- Wrote condition reports and answered customer inquiries by phone and email
- Catalogued work in RFC auction systems and lotted work for sale on Invaluable.com
- Installed 100+ pieces for sale in monthly auctions and took live phone bids

Smithsonian National Portrait Gallery (NPG) | Exhibition Design Intern | Washington, DC | 2015

- Maintained 50,000+ ft^2 of gallery space including signage, graphics, sculpture, and framed works
- Created mounts for Alexander Gardner photographs and stereocards in the Lunder Conservation Lab
- Installed 40+ objects and gallery elements for the NPG One Life: Dolores Huerta exhibition
- Worked with NPG registrar to store, frame, crate, and ship artwork

Strathmore Hall Foundation | Visual Arts Intern | Rockville, MD | 2014

- Wrote and edited curator statements, exhibition literature, and gallery signage
- Trained docents, managed community artist membership program and children's summer art camp

Arts Leadership

RISD Museum Guild | Providence, RI | 2015-2018

- Collaborated with Guild members to create, advertise, and execute monthly student programming

- Created gallery talk on Richard Artschwager's *Chair/Table* for a general audience

Brown University Student Creative Arts Council | Providence, RI | 2015-2018
- Curated, advertised, and installed annual student art exhibitions at the Granoff Center for the Arts
- Juried $15,000 Student Grant program annually

Brown University Aerial Arts Society | Providence, RI | 2013-2018
- President of a 50+ member student aerial dance and circus arts group
- Scheduled biweekly rehearsals and taught aerial hoop classes to 20+ beginners weekly
- Directed, choreographed, and performed in biannual acrobatics showcases
- Coordinated with campus administration and OSHA to ensure rigorous structural safety practices

Science Communication and Outreach

Medill School of Journalism| Skills & Careers in Science Writing | Evanston, IL 2019
- Trained in effective distillation of complex scientific concepts for a general audience

Science in the Classroom | Volunteer | Chicago, IL 2019
- Lead science lab demonstrations for 3rd grade students at Hayt elementary school

Teaching Experience

Northwestern University | Graduate Teaching Assistant | Evanston, IL | 2018-2021
- Taught and supervised 100+ undergraduate students in organic chemistry lab
- Provided one-on-one feedback to students on methodology and scientific reasoning skills

Rhode Island School of Design | Undergraduate Teaching Assistant | Providence, RI | 2014-2015
- Set up vignettes and posed figure models
- Contributed to teacher's comments during critique
- Researched and wrote course materials

Awards and Recognitions

2015 **Drawing Served** | Featuring "The Infinite Directions of the Body"
2014 **RISD Portfolios** | Featuring "The Infinite Directions of the Body"

Publications

3. Brown, A. M., **Butman, J. L.,** Lengacher, R., Vargo, N. P., Martin, K. E., Koller, A., Śmiłowicz, D., Boros, E., Robinson, J. R. "*N,N*-Alkylation Clarifies the Role of *N*- and *O*-protonated Intermediates in Cyclen-based ^{64}Cu Radiopharmaceuticals" *Inorg. Chem.* (2022)
2. **Butman, J. L.**; Thomson, R.; Geiger, F. "Unanticipated Hydrophobicity Increases of Squalene and Human Skin Oil Films Upon Ozone Exposure" *J. Phys. Chem. B.* (2022)
1. von Domaros, M.; Liu, Y.; **Butman, J. L.**; Perlt, E.; Geiger, F.; Tobias, D. "Molecular Orientation at the Squalene:Air Interface from Sum Frequency Generation Spectroscopy and Atomistic Modeling" *J. Phys. Chem. B.* (2020)

Presentations

5. *Oral:* **J. Butman.** "Hydrophobic Material from Heterogeneous Ozonolysis of Human Skin Oil." Northwestern University 3rd Year Organic Chemistry Seminar Series, June 2021.
4. *Oral:* F. Geiger; Y. Liu; **J. Butman.** "Surface Chemistry and Transformations of Indoor Molecular, Nano-, and Microlayers." SURF-CIE meeting, January 2020.
3. *Oral:* **J. Butman.** "Love is Temporary, Things are Forever." The Brown|RISD Dual Degree Class of 2018 Capstone Presentations, May 2018.
2. *Poster:* **J. Butman.** "Synthesis of Novel Cyclic Ammonium DO_3A Compounds and their Metal Complexes." Department of Chemistry Brown University Undergraduate Poster Session, April 2018.
1. *Oral:* **J. Butman.** "Cleaning Methods for Audio Carriers." Library of Congress Junior Fellows Display Day, August 2017.

Exhibitions

2018 **Sit on It: Furniture Senior Show 2018** | Woods-Gerry Gallery, Providence, RI.
2018 **X: The 10th Annual Brown|RISD Dual Degree Exhibition** | Granoff Center for the Arts, Providence, RI.
2017 **Intermission/Intervention/Interruption** | RISD Museum, Providence, RI. **Curator.**
2017 **Spring Arts Festival** | Granoff Center for the Arts, Providence, RI. **Curator.**
2016 **2"x4": The 8th Annual Brown|RISD Dual Degree Exhibition** | Granoff Center for the Arts, Providence, RI.
2015 **Of[f] Course: The 7th Annual Brown|RISD Dual Degree Exhibition** | Granoff Center for the Arts, Providence, RI.
2015 **Spring Arts Festival** | Granoff Center for the Arts, Providence, RI.